Inhibition of Cellular MEK/ERK Signaling Suppresses Murine Papillomavirus Type 1 Replicative Activities and Promotes Tumor Regression

Adrian J. Luna[a,1], Jesse M. Young[a, 2], Rosa T. Sterk[a], Virginie Bondu[a], Fred A. Schultz[b], Donna F. Kusewitt[b,d], Huining Kang[c,d], Michelle A. Ozbun[a,d,*]

[a] Department of Molecular Genetics & Microbiology, The University of New Mexico School of Medicine, Albuquerque, NM 87131

[b] Department of Pathology, The University of New Mexico School of Medicine, Albuquerque, NM 87131

[c] Department of Internal Medicine, Division of Epidemiology, Biostatistics and Preventive Medicine, The University of New Mexico School of Medicine, Albuquerque, NM 87131

[d] The University of New Mexico Comprehensive Cancer Center, Albuquerque, NM 87131

[1] Present address: University of Michigan, Ann Arbor, MI 48109

[2] Present address: TriCore Reference Laboratories, Albuquerque, NM 87102

* Corresponding Author: Michelle A. Ozbun

Email: mozbun@salud.unm.edu

Author Contributions: Author contributions: A.J.L., J.M.Y., and M.A.O. designed research; A.J.L., J.M.Y., R.T.S., and V.B. performed research; A.J.L., J.M.Y., F.A.S., D.F.K., H.K., and M.A.O. analyzed data; and A.J.L., J.M.Y., and M.A.O. wrote the paper.

Competing Interest Statement: The authors declare no competing interests.

Keywords: papillomavirus, tumorigenesis, MEK signaling, trametinib, cobimetinib

This PDF file includes:

Main Text
Figures 1 to 4
Table 1

Abstract

Human papillomaviruses (HPVs) are a significant public health concern due to their widespread transmission, morbidity, and oncogenic potential. Despite efficacious vaccines, millions of unvaccinated individuals and those with existing infections will develop HPV-related diseases for the next two decades. The continuing burden of HPV-related diseases is exacerbated by the lack of effective therapies or cures for most infections, highlighting the need to identify and develop antivirals. The experimental murine papillomavirus type 1 (MmuPV1) model provides opportunities to study papillomavirus pathogenesis in cutaneous epithelium, the oral cavity, and the anogenital tract. However, to date the MmuPV1 infection model has not been used to demonstrate the effectiveness of potential antivirals. We previously reported that inhibitors of cellular MEK/ERK signaling suppress oncogenic HPV early gene expression *in vitro*. Herein, we adapted the MmuPV1 infection model to determine whether MEK inhibitors have anti-papillomavirus properties *in vivo*. We demonstrate that oral delivery of a MEK1/2 inhibitor promotes papilloma regression in immunodeficient mice that otherwise would have developed persistent infections. Quantitative histological analyses revealed that inhibition of MEK/ERK signaling reduces E6/E7 mRNAs, MmuPV1 DNA, and L1 protein expression within MmuPV1-induced lesions. These data suggest that MEK1/2 signaling is essential for both early and late MmuPV1 replication events supporting our previous findings with oncogenic HPVs. We also provide evidence that MEK inhibitors protect mice from developing secondary tumors. Thus, our data suggest that MEK inhibitors have potent anti-viral and anti-tumor properties in a preclinical mouse model and merit further investigation as papillomavirus antiviral therapies.

51 **Significance Statement**

52 Persistent human papillomavirus (HPV) infections cause significant morbidity and oncogenic HPV
53 infections can progress to anogenital and oropharyngeal cancers. Despite the availability of effective
54 prophylactic HPV vaccines, millions of unvaccinated individuals, and those currently infected will develop
55 HPV-related diseases over the next two decades and beyond. Thus, it remains critical to identify effective
56 antivirals against papillomaviruses. Using a mouse papillomavirus model of HPV infection, this study
57 reveals that cellular MEK1/2 signaling supports viral tumorigenesis. The MEK1/2 inhibitor, trametinib,
58 demonstrates potent antiviral activities and promotes tumor regression. This work provides insight into the
59 conserved regulation of papillomavirus gene expression by MEK1/2 signaling and reveals this cellular
60 pathway as a promising therapeutic target for the treatment of papillomavirus diseases.

61
62
63

Main Text

Introduction

Human papillomavirus (HPV) infections are highly prevalent and cause a variety of epithelial neoplasms (i.e., tumors) ranging in severity from benign cutaneous warts to precancerous intraepithelial neoplasia to cancers (1). Over 200 HPV genotypes have been identified and sequenced (2) with low-risk mucosotropic HPVs causing 90% of anogenital warts and all laryngeal papillomas and high-risk HPV infections etiologically linked to anogenital and oropharyngeal cancers (3). Despite effective prophylactic vaccines, millions of unvaccinated people and those with existing infections are projected to develop HPV-related diseases for the next two decades (4) and beyond (5). Current HPV treatments involve lesion excision or ablation, cryotherapy, chemotherapy, and radiation, each risking long-term morbidities with reduced quality of life (6-9). Additionally, recurrence rates for some treatments can be >50% (10, 11). To date, there are no effective antiviral HPV therapies and no cure for most HPV infections.

Like all PVs, HPVs are highly host specific and cannot be productively transmitted to animals. Although this has inhibited detailed studies of HPV pathogenesis and immunology, experimental infections using a variety of vertebrate animal PVs have provided valuable models for understanding viral gene functions, tissue tropism, regression and persistence, cancer progression, vaccine efficacy, and potential therapeutic agents (12). Despite differences in epithelial tropisms and disease manifestations, mammalian PVs have similar genome organization, protein functions, and reliance on epithelial differentiation for productive replication (1). The murine PV type 1 (MmuPV1) mouse model is a major advancement in preclinical models of PV-induced infection and disease (13). Whereas mouse models are frequently used to identify and test candidate interventions and the MmuPV1 should be a valuable preclinical model, to our knowledge, this model has not been used to demonstrate the efficacy of antiviral agents.

In all mammalian PVs, tumorigenesis is primarily driven by the E6 and E7 proteins (14, 15). Although E6 and E7 from different PV genera interact with different cellular targets, E6 and E7 expression reprograms cells in the para- and supra-basal layers to maintain cell cycle progression and proliferative capacity (14, 16, 17). This promotes a cellular environment where viral genomes are amplified for packaging by the

92 capsid proteins into new virions (16). Additionally, E6 and E7 proteins play critical roles in viral genome
93 maintenance and amplification to support productive PV infections (18, 19). As E6 and E7 proteins are the
94 key factors for PV persistence and oncogenesis, they are frequently considered to be ideal therapeutic
95 targets (20, 21). Genetic knockdown of oncogenic HPV E6 and E7 expression restores cell cycle
96 checkpoint (e.g., p53 and pRb) functions, inhibits cell proliferation, and leads to cellular apoptosis and/or
97 senescence (22-30). Yet, genetic approaches have not been robustly adaptable to human clinical studies.
98 A handful of small molecules have been investigated for their abilities to inhibit PV protein activities (31),
99 but none so far show promise *in vivo*.

100 We recently reported that cellular MEK/ERK signaling is a key modulator of high-risk HPV E6/E7
101 transcription (32). The RAS-RAF-MEK-ERK signaling pathway is evolutionarily conserved, has been
102 extensively investigated in mammalian cells, and is the best understood signaling cascade in tumor cell
103 biology (33). MEK signaling is tightly controlled in normal epithelium where proliferative signals from
104 growth factor receptors are restricted to promote epithelial homeostasis, including cellular contact inhibition
105 and differentiation (34-37). Thus, MEK signaling is normally limited to the lower epithelial cell layers. MEK
106 signaling is effected by the MEK1 and MEK2 isoforms, which are structurally similar and share activation
107 mechanisms. Upon activation by RAF, they function as dual-specificity tyrosine and serine/threonine
108 kinases, phosphorylating their only known *in vivo* substrates ERK1 and ERK2 on specific tyrosine and
109 threonine residues (38). MEK1 and MEK2 exhibit extensive functional redundancy and form functional
110 homo- or hetero-dimers *in vivo* (39). However, increasing evidence suggests that MEK1 and MEK2 have
111 distinct activities that may be controlled by specific modulation of their activity levels (40, 41), differential
112 binding to cellular proteins (42-46) and disparate outcomes when the genes are knocked out in mice (39,
113 47, 48). Despite an incomplete understanding of the distinct functions of MEK1 and MEK2, particularly in
114 the epithelium, MEK/ERK activation has long been recognized to play a key role in cell proliferative
115 diseases and neoplastic progression. For example, p-ERK1/2 levels are increased in the upper epithelial
116 layers in several proliferative skin diseases, including HPV-driven cervical neoplasia (49). We found, in a
117 cohort of 580 biopsies from normal cervix, low-, and high-grade cervical intraepithelial neoplasia (CIN), a
118 significant correlation ($p<0.001$, $X^2=212.7$) between increasing levels of p-ERK and E7 protein activity

119 during disease progression (32). Mechanistically, using high-risk HPV-infected 3D organotypic (raft)
120 epithelial tissues and monolayer cultures, we showed that MEK-induced phosphorylation of ERK1/2
121 robustly governs HPV E6/E7 mRNA transcription. Importantly, we demonstrated that small molecule
122 inhibitors of MEK and ERK potently inhibit HPV E6/E7 transcription, at least in part by blocking the
123 activation of activator protein-1 (AP-1) transcription factors (32) whose binding sites are conserved in the
124 long control region (LCR) enhancer/promoter of all PV genomes (50).

125 The combined conservation of PV genome structure, epithelial differentiation-dependent PV gene
126 regulation, and MEK/ERK signaling in mammalian epithelium prompted us to hypothesize that inhibitors of
127 MEK signaling would suppress E6/E7 gene transcription and tumor growth in the preclinical MmuPV1-
128 induced tumor model that recapitulates key aspects of HPV-induced tumorigenesis (13). We investigated
129 two FDA- and European Medicines Agency-approved MEK inhibitors, trametinib and cobimetinib (51).
130 Both drugs have similar *in vitro* inhibitory concentration 50 (IC_{50}) efficacies for preventing activation of
131 MEK1 (0.7 nM and 0.95 nM, respectively) and trametinib is equivalently inhibitory of the MEK2 isoform
132 (IC_{50} = 0.9 nM). However, cobimetinib is ≈200-fold less potent against MEK2 (IC_{50} = 199 nM) (51). After
133 inducing tumors on the tails of Hsd:Athymic-*FoxN1*^{nu} mice that lack T cells, mice were treated orally with
134 drug dosages based on previous studies (51). Both drugs effectively inhibited tumor growth, but trametinib
135 led to significant tumor regression beginning about 1 week post treatment initiation. Furthermore, the MEK
136 inhibitors prevented overt lesion formation at secondary sites, suggesting diminished MmuPV1
137 transmission. Both drugs display mechanisms of action consistent with reduced viral gene expression and
138 genome replication and suppressed cellular proliferation as expected from our prior *in vitro* study (32).
139 Our results strongly suggest that both MEK1 and MEK2 are important for PV tumorigenesis, and that
140 further investigations of MEK1/2 inhibitors are warranted for the treatment of PV-induced diseases in
141 humans and animals.

142
143
144

145 **Results**
146
147 **MEK Inhibitors Suppress MmuPV1-Induced Tumor Growth and Reduce Papillomatous Morphology.**
148 After MmuPV1 inoculation and 6 weeks of papilloma growth, mice were randomized into treatment groups;
149 the average tumor volume of each group was ≈40 mm^3 (Fig. 1A) with no significant size differences among
150 the groups (*SI Appendix* Table 1). Mice were orally administered either vehicle, the MEK1 inhibitor
151 cobimetinib (7.5 mg/kg or 15 mg/kg), or the MEK1/2 inhibitor trametinib (1.0 mg/kg or 2.0 mg/kg) every 2
152 days. As visualized in Fig. 1B, C and detailed in *SI Appendix* Table 1, tumor volumes significantly differed
153 among the five groups after 8 days of treatment (p=0.042) and the difference became increasingly
154 pronounced as time passed. Over the 30-day treatment period, tumors of vehicle-treated mice increased
155 in size by an average of 2.59-fold, resulting in a final average tumor volume of 101.7 mm^3. Comparatively,
156 mice treated with 7.5 mg/kg or 15 mg/kg of cobimetinib demonstrated significantly impaired papilloma
157 growth resulting in final average tumor volumes of 42.4 mm^3 (58% TGI) and 45.4 mm^3 (55% TGI),
158 respectively (*SI Appendix* Table 1). More strikingly, trametinib treatment resulted in papilloma regression
159 over the same period, reducing tumor volumes to an average of 25.0 mm^3 for 1 mg/kg trametinib and 25.2
160 mm^3 for 2 mg/kg trametinib (both 75% TGI; *SI Appendix* Table 1). Pairwise comparisons revealed
161 significant differences between vehicle-treated and each of the drug treatment groups (adjusted p-value
162 <0.05), but no significant differences when comparing each of the four groups that received the MEK
163 inhibitors (*SI Appendix* Table 2). Similarly, the rates of tumor volume change (mm^3/day) among the
164 treatment groups estimated by linear mixed-effects model analysis showed that the vehicle-treatment
165 group significantly increased over time while the trametinib-treated groups significantly decreased, and the
166 cobimetinib-treated groups did not have a significant change (*SI Appendix* Table 3). Furthermore,
167 trametinib demonstrated significant superiority over cobimetinib in promoting tumor regression as
168 demonstrated by comparing the rates of tumor volume change among the MEK inhibitor treated groups
169 (p-value = 0.0334; *SI Appendix* Table 4). The visual characteristics of the tail papillomas on mice treated
170 with MEK inhibitors were distinct compared to papillomas on vehicle-treated mice (Fig. 1D; *SI Appendix*
171 Fig. S1). Specifically, vehicle-treated mice bore florid and irregular papillomas. Whereas mice treated with
172 both cobimetinib doses exhibited smaller tumors with less florid appearance, mice treated with both

173 trametinib doses generally displayed more flattened and smoother papillomas (Fig. 1D; *SI Appendix* Fig.
174 S1). Note that only one animal, in the high dose trametinib treatment group, showed significant weight loss
175 suggesting toxicity (*SI Appendix* Fig. S1F-H). These data indicate that MEK inhibitors have profound TGI
176 effects *in vivo* using the MmuPV1 preclinical model; compared to the MEK1 inhibitor cobimetinib, the
177 MEK1/2 inhibitor trametinib, demonstrated superior TGI.

178

179 **MEK Inhibitor Effects on Tissue Morphology and Cellular Biomarkers.** Serial, sagittally sectioned
180 tails were analyzed histologically after H&E staining, focusing on the mice treated with vehicle and those
181 treated with the higher doses of the two MEK inhibitors (Fig. 2A; *SI Appendix* Fig. S2). Papillomas from
182 vehicle-treated mice showed extensive fibrillary projections throughout the tumor cross-sections. In drug-
183 treated mice, particularly those treated with the MEK1/2 inhibitor, trametinib, the extent of papillary
184 projections was considerably reduced (Fig. 2A). Consistent with this observation, morphometric analyses
185 of all tumors revealed significantly reduced epithelial thickness in the papillomas from mice treated with
186 the MEK inhibitors compared to vehicle-treated mice (Fig. 2B). Tumor sections from all three groups
187 revealed dysplastic epithelium and hyperkeratosis, albeit with noticeable differences depending upon the
188 treatment (*SI Appendix* Fig. S2). Koilocytes, epithelial cells characterized by perinuclear haloes
189 (cytoplasmic vacuolation) surrounding condensed nuclei, are pathognomonic of HPV infections (52) and
190 were scattered irregularly throughout the differentiating epithelium in all MmuPV1 lesions.

191 The MEK inhibitors suppressed the levels of phosphorylated-ERK1/2 (p-ERK1/2), the only recognized
192 signaling effector of MEK, in the tumors (Fig. 2C-D); moreover, p-ERK1/2 levels have a strong correlation
193 with tumoral epithelial lesion thickness ($r=0.7151$, $p=0.00185$; *SI Appendix* Fig. S5A). p-ERK1/2 was most
194 prominent in the papillomas of vehicle-treated mice, localizing primarily to basal and lower suprabasal
195 layers of all papillomas. These data indicate that the systemically delivered MEK inhibitors reached the tail
196 epithelium to suppress MEK/ERK signaling. Further, the findings suggest that MEK signaling is an
197 important contributor to papilloma growth and maintenance in the MmuPV1 mouse model.

198 As MEK/ERK signaling is integral to epithelial proliferation and differentiation (53), we evaluated the
199 papillomas for differentiation-associated epithelial markers, keratin 5 (K5) and keratin 10 (K10). K5 pairs
200 with K14 and these proteins are characteristic of mitotically active, undifferentiated basal cells of the
201 epithelium; their expression is downregulated as cells begin to differentiate (54). In contrast, K10 is an
202 established early marker of keratinocytes entering terminal differentiation (55). As expected, strong K5
203 staining was prominent in the cells nearest the basement membranes of all tumors. The vehicle-treated
204 mice displayed an expansive network of undifferentiated cells throughout the thickness of the fibrillary
205 papillomas (Fig. 2E; *SI Appendix* Fig. S3A-D), as previously reported for MmuPV1 tail lesions (17).
206 However, MEK inhibitors counteracted basal cell expansion and the number of K5-positive cells was
207 reduced (Fig. 2F) and were correlated with p-ERK1/2 levels (r=0.5947, p=0.0249) and strongly correlated
208 with lesion thickness (r=0.7641, p=0.000569; *SI Appendix* Fig. S5B-C, respectively). Likewise, the number
209 of differentiating K10-positive cells was significantly lower in the smaller papillomatous lesions of the drug-
210 treated mice compared to those in vehicle-treated mice (Fig. 2G-H). Interestingly, there were no significant
211 differences amongst the treatment groups in the percentages of lesional cells that expressed p-ERK1/2,
212 K5, or K10 (*SI Appendix* Fig. S3E-G). These findings indicate that while MEK inhibition and suppressed p-
213 ERK1/2 signaling reduced the number of proliferative cells, there were no net changes in the overall
214 proportion of cells proliferating or differentiating within the papillomas.

215 Infection with MmuPV1 or oncogenic HPVs leads to increased expression of Ki67, a basal cell proliferation
216 marker (56-59) and Sundberg et al. showed similar staining patterns between Ki67 and K5 in MmuPV1-
217 induced tail tumors (56). Furthermore, MEK inhibition is known to reduce Ki67 staining in epithelial tumors
218 (60, 61). Although we attempted to detect Ki67 by immunohistochemistry (IHC) in the tumor sections, we
219 were unable to obtain quantifiable Ki67 staining. This is likely because tissue decalcification has been
220 found to impair the detection of nuclear biomarkers (62).

221

222 **MEK Inhibitor-Induced Papilloma Regression does not Involve T Cells or Neutrophils.** Whereas
223 various data indicate that CD4+ and CD8+ T cells play a major role in papillomavirus-induced lesion

224 regression (56, 63-66), there also are indications that neutrophils might contribute to MmuPV1 disease
225 control in immunocompetent models (67). As the Hsd:Athymic-*FoxN1*^{nu} mice used in this investigation
226 lack CD4+ and CD8+ T cells but have an intact innate immune system, we investigated if MEK inhibition
227 resulted in increased neutrophil infiltration in the MmuPV1-induced papillomas. Quantification of tumor-
228 proximal myeloperoxidase staining revealed no significant differences in neutrophil infiltration amongst
229 treated and control papillomas (Fig. 3A-B). Thus, the data suggest that MEK inhibitors suppressed tumor
230 growth and trametinib promoted regression *via* a mechanism independent of T cells and neutrophils.

231

232 **The MmuPV1 Vegetative Replication Cycle is Dependent on MEK Signaling.** Our recent publication
233 demonstrated that HPV early gene expression relies on MEK/ERK signaling and that MEK1/2 inhibition
234 results in reduced viral early gene transcription and protein expression (32). As robust PV genome
235 amplification leading to late gene expression depends on sufficient PV early gene expression (18, 19, 68),
236 we determined the effect of MEK inhibition on key aspects of the complete MmuPV1 replicative cycle. We
237 first strove to quantify the tumor levels of E6/E7 oncogene mRNA, which should be present predominantly
238 in the cytoplasm of infected epithelium (Fig. 3C). Despite various DNase treatment methods to remove
239 viral genomes, the E6/E7 probes consistently bound to nuclear targets, particularly evident in the vehicle-
240 only tumors (*SI Appendix* Fig. S4A). Thus, the data in Fig. 3C-D likely represent detection of MmuPV1
241 genomes and E6/E7 mRNAs; yet the morphometric analyses demonstrate the MEK inhibitors significantly
242 reduced the levels of MmuPV1 nucleic acids in the tumors. Consistent with this interpretation, the *in situ*
243 hybridization (ISH) probe specific to the MmuPV1 noncoding long control region (LCR), revealed ISH
244 staining patterns with obvious overlap in serial sections (Fig. 3, compare panels C and E; *SI Appendix* Fig.
245 S4). Morphometric quantification of ISH data showed overall lower levels of LCR-targeted viral genomes
246 compared to the E6/E7 ISH results in each treatment group (Fig. 3F and D, respectively). There was a
247 strong correlation between E6/E7 ISH and LCR ISH ($r=0.9263$, $p<0.00001$; *SI Appendix* Fig. S5J).
248 Furthermore, both RNA ISH and DNA ISH levels had strong correlations with p-ERK1/2 levels ($r=0.8303$,
249 $r=0.7421$, both $p<0.001$; *SI Appendix* Fig. S5E-F, respectively). Together, the data indicate significantly

250 decreased viral genome levels and imply reduced E6/E7 mRNAs in tumors from mice receiving the MEK
251 inhibitors. Lastly, IF detection of MmuPV1 major capsid protein L1 along with K14 staining of
252 undifferentiated basal cells in the tumor sections revealed significantly fewer L1-positive foci in the
253 differentiating layers of tumors of the cobimetinib and trametinib treatment groups (Fig. 3G,H). Additionally,
254 E6/E7 and viral LCR ISH were strongly correlated with L1-foci ($r=0.7245$, $p<0.0015$ and $r=0.8411$,
255 $p<0.0001$; *SI Appendix* Fig. S5L-M, respectively). These data clearly support the idea that the MEK
256 inhibitors suppressed the MmuPV1 replicative cycle *in vivo*.

257

258 **MEK Inhibitor Treatment Reduces MmuPV1 Transmission *in vivo.*** Over the treatment course, we
259 observed that all (6/6) vehicle-treated mice developed papillomas on their muzzles (Fig. 4A; Table 1). In
260 contrast, the only mouse from the MEK inhibitor treatment cohorts to develop a visible facial wart (1/24)
261 was in the group receiving the lower dose (7.5 mg/kg) of cobimetinib (Table 1). This mouse was co-housed
262 with other animals receiving cobimetinib (i.e., it was not co-housed with vehicle-treated mice). H&E staining
263 and E6/E7 ISH confirmed that the facial lesions arose from MmuPV1 infections (Figure 4B). As the snouts
264 were not experimentally scarified or infected, the secondary muzzle-arising infections were likely
265 transmitted from tail grooming. The most obvious explanation for lack of secondary muzzle infections in
266 MEK inhibitor-treated mice is that their tail papillomas produced fewer virions due to suppressed viral
267 replication as shown in Fig. 3C-H. We reported that MEK/ERK signaling stimulates HPV early gene
268 expression *via* activation of cellular fos/jun family transcription factors (32), which bind to AP-1 binding
269 sites that are highly conserved in papillomavirus LCRs (69). Thus, it is also possible that MEK inhibition
270 would result in lower viral early gene transcription after infection-mediated delivery of viral genomes to the
271 cell nucleus. To test this prospect, we exposed HaCaT keratinocytes to MmuPV1 virions in the presence
272 of increasing doses of trametinib. Indeed, MEK inhibition resulted in significantly decreased levels of
273 spliced MmuPV1 E1^E4 mRNAs compared to vehicle treated cells (Fig. 4C). Combined, our data suggest
274 that MEK inhibition is likely to impede new MmuPV1 infections by both reducing virion shedding from
275 existing lesions and by suppressing early viral transcription during infection establishment at new sites.

276
277 **Discussion**
278
279 Herein we demonstrate both the important role for MEK1/2 signaling in PV-induced tumorigenesis and the
280 potent antiviral and tumor suppressive properties of MEK1/2 inhibitors in a preclinical, natural infection
281 model of HPV disease. This work confirms and extends our recent study showing that inhibiting MEK/ERK
282 signaling has antiviral effects, specifically reducing early gene transcription and oncoprotein functions,
283 against oncogenic HPVs in three dimensional organotypic epithelial tissue cultures (32). The conservation
284 of MEK/ERK signaling in mammalian epithelium coupled with the conservation of MEK/ERK activated AP-
285 1 transcription factor binding sites in the LCRs of animal PVs indicates that this pathway is both critical for
286 controlling PV early gene transcription and a prime target for PV antivirals. Thus, our work suggests that
287 targeting this pathway is likely to have antiviral effects for all mammalian PV infections. Importantly, in our
288 prior work and in this study, the antiviral and tumor suppressive effects of MEK inhibitors on PV infections
289 occurred in the absence of T cells, which has significant clinical implications for treating PV infections in
290 individuals lacking functional T cells.

291 An important aspect of our study that is particularly relevant to treating pathogenic HPV induced lesions is
292 the fact that we initiated treatments only after MmuPV1 infection induced clinically evident papillomas
293 (average of ≈40 mm^3 in each cohort) six weeks post inoculation. Most preclinical studies designed to test
294 candidate therapies against PV disease begin treatments prior to pathologically confirmed disease. For
295 example, a study investigating the antiviral effects of dihydroartemisinin (DHA, an active metabolite of
296 artesunate) showed topical treatment could inhibit the development of mucosal tumors in two of three
297 animals exposed to canine oral papillomavirus (70). However, the treatment was initiated 24h after viral
298 challenge and ≈3 weeks prior to tumor development in the vehicle-treated animals. More recently, DHA
299 was tested following MmuPV1 challenge in the murine anal or cervicovaginal tract; however, neither the
300 persistence of viral infections nor the presence of disease was verified at these sites prior to treatment
301 initiation (71). Even so, DHA failed to reduce disease development at either site. This was surprising given
302 that topical vaginal delivery of artesunate led to histologic regression in 19/28 (67.9%) of
303 immunocompetent women with HPV-induced CIN grade 2/3 and HPV clearance in 9/19 (47.4%) subjects

304 whose lesions underwent histologic regression (72). A recent report typifies the strategies of testing
305 therapeutic HPV vaccines. Mice were subcutaneously injected with HPV16 E6/E7 expressing TC-1 tumor
306 cells, which expanded to a 9 to 12 mm^2 area within 10 to 12 days, respectively, and then given a single
307 intramuscular dose of mRNA-lipid nanoparticle vaccines encoding a fusion protein of the type 1 herpes
308 simplex virus glycoprotein D and HPV16 E7 protein (73). The treatments led to regression in 4/5 (80%)
309 and 4/7 (60%) of the respective cohorts; however, there was no indication that the sites of tumor growth
310 were analyzed for residual HPV-positive tumor cells. Thus, our approach to testing established PV lesions
311 in this study more closely represents clinically relevant HPV disease, making our tumor regression results
312 particularly remarkable.

313 A major strength of this study is the use of pathologist-guided, quantitative tumor tissue analyses of tumor
314 thickness and a battery of biomarkers relevant to PV-induced tumorigenesis. Coupled to robust statistical
315 analyses, our objective quantification of biomarkers reveals clearly that MEK inhibitors accessed the
316 MmuPV1-infected epithelium to suppress p-ERK1/2 levels, basal cell expansion, and tumor
317 thickness/volume without affecting overall epithelial differentiation. Whereas it is most likely that MEK
318 inhibition suppressed tumor growth *via* both blunting ERK-mediated cellular proliferative signals and
319 reducing the transcription of MmuPV1 early genes that promote cell proliferation, the precise contribution
320 of each of these interdependent activities to the overall decreased tumor growth will be challenging to
321 dissect.

322 The MmuPV1 tumor growth inhibitory effect of the MEK1/2 inhibitor, trametinib, was superior to that of
323 cobimetinib, which preferentially targets the MEK1 isoform. Despite the functional redundancy of MEK1
324 and MEK2 in many assays (39), our understanding of their distinct activities and differential regulation is
325 expanding. For example, MEK1 contains a site (Thr292) for ERK-mediated feedback phosphorylation
326 whereas MEK2 lacks this site (40, 41). Additionally, several scaffold proteins specifically bind to and
327 enhance the activation of MEK1, but not MEK2 (42-45). MEK1 knockout in mice is embryonic lethal (39,
328 47), whereas MEK2 knockout animals are viable, fertile, and phenotypically normal (48). MEK2, but not
329 MEK1, phosphorylates the tumor suppressor GCIP (Grap2- and cyclin D1-interacting protein), promotes

330 its degradation, and decreases its tumor suppressor function (46). Our work strongly suggests that
331 inhibition of both MEK1 and MEK2 is crucial for controlling PV disease. However, MEK2 appears to have
332 distinct functions important for MmuPV1 tumor growth that will require futher dissection. There could
333 certainly be other biologicial explanations for the greater potentcy of trametinib.

334 The ability of MEK1/2 inhibition by trametinib to promote tumor regression became evident only four days
335 post treatment, when the mean tumor volumes in the drug-treated groups were smaller than the group's
336 mean starting tumor volumes (Fig. 1C, *SI Table 1*). While the tumors in the trametinib-treated groups
337 continued to decrease in size over the next two weeks, the growth reduction seemed to plateau thereafter.
338 This raises important questions as to whether continued trametinib treatment would eventually cure the
339 infections, or whether the drug had reached its maximum effects. It seems likely that ceasing treatment
340 with the drugs prior to complete MmuPV1 clearance would result in regrowth of the tumors, but this has
341 yet to be tested and it would also be informative to do so in the context of functional T cells.

342 The mechanisms by which the MEK inhibitors exerted their effects in this MmuPV1 infection and
343 tumorigenesis model are consistent, in part, with those observed in other non-PV-related cancer models.
344 In a variety of cancer cell types *in vitro*, trametinib and cobimetinib have been shown to reduce p-ERK1/2,
345 modulate cyclin D1 and p27 levels in a manner aligned with a G1/S cell cycle arrest, and induce caspase-
346 dependent apoptosis (61, 74, 75). Unfortunately, a limitation of our study was the inability to detect nuclear
347 antigens in the lesions due to Versenate treatment for tail decalcification before fixation. Because
348 Sundberg et al. showed similar staining patterns between Ki67 and K5 in MmuPV1-induced tail tumors
349 (56), and we found a correlation between p-ERK1/2 levels and strong K5 staining ($r=0.5947$, $p=0.025$; Fig.
350 S5B), we infer that MEK inhibitors suppressed cellular proliferation. Additionally, the strong correlations
351 between p-ERK1/2 levels and MmuPV1 E6/E7 mRNA ($r=0.8303$, $p= 6.85e-5$) and between strong K5
352 staining and MmuPV1 E6/E7 mRNA ($r=0.8202$, $p=9.995e-5$) highlight the interdependency of the
353 biomarkers p-ERK1/2, K5 and MmuPV1 E6/E7 mRNA transcription (Fig. S5B, E, I). Future studies
354 evaluating cellular markers of proliferation, apoptosis, and senescence will be needed to clearly delineate
355 the antiproliferative effect of MEK inhibition in mammalian PV tumors.

356 In our previous study and in this work, the antiviral and tumor suppressive effects of MEK inhibition
357 occurred in the absence of T cells (32). This has important clinical implications for treating PV diseases in
358 those who are immunocompromised (76). For example, people living with AIDS have increased HPV
359 acquisition, prevalence, persistence, high tumor burdens, and cancer progression (77) and would greatly
360 benefit from effective HPV antiviral treatments. Herein, neither T cells nor neutrophils were implicated
361 tumor regression despite reports that immune mediated cell death is an important characteristic of tumor
362 reduction (reviewed in (78)). Whether immune cell populations are involved in the MEK-inhibitor induced
363 regression of PV neoplasia will require further investigation. Importantly, use of MEK1/2 inhibitors as a
364 therapeutic for PV diseases must be tested in the context of functional T cells as MEK signaling is induced
365 by T cell receptor signaling (79). While this could be a disadvantage to tumor clearance, recent evidence
366 indicates that MEK inhibitors can lead to a shift from a Th2 to a Th1 response (80), a reduction of regulatory
367 T cells (81), and reprogramming of CD8+ T cells into memory stem cells with antitumor activities (82), each
368 of which might further benefit treatment of PV diseases. Lastly, we provide strong evidence that MEK
369 inhibitors reduced productive MmuPV1 infection measured by both the reduced levels of the viral capsid
370 protein, L1 in tumors, and the lack of secondary muzzle infections observed in the MEK inhibitor-treated
371 mice. In total, our work strongly suggests that MEK1/2 inhibitors warrant further investigation for treatment
372 of mammalian PV infections *in vivo*; such an approach might also reduce PV transmission to new
373 susceptible epithelial sites or between individuals.

374 **Materials and Methods**
375
376 **MmuPV1 infections, tumor growth and treatments.** All animal work was approved by the University of
377 New Mexico's IACUC (protocol #20-201020-HSC). Female Hsd:Athymic Nude-*Foxn1*^{nu} outbred mice
378 (Envigo) 6-8 weeks of age were inoculated with MmuPV1 virions (a kind gift from Prof. Paul Lambert, Univ.
379 of Wisconsin-Madison). Specifically, the mice were anesthetized and maintained in anesthesia using 3%
380 isoflurane in O_2. Prior to inoculation, the tail of each mouse was scarified using a 27.5-gauge needle. To
381 standardize infection area and papilloma growth the scarification was initiated 0.5-cm distal to the tail base
382 and continuing for 1-cm toward the tip. Each mouse tail was superficially scarified by scratching over the
383 epithelial surface 20-30 times as described (83). Scarification and viral inoculations were carried out in a
384 biosafety cabinet. MmuPV1 virions ($2x10^8$ viral genome equivalents [VGE] in 2 µl) were applied across
385 the entirety of each wound site using a siliconized pipette tip. The MmuPV1 inocula were allowed to
386 penetrate the wound before returning mice to microisolator (biocontainment) cages. Mice were monitored
387 weekly for weight and the appearance of warts. Tumor volumes were determined with digital calipers (Bel-
388 Art Products) using the formula (length*width*height): length was measured from the sagittal plane, width
389 from the transverse plane, and height was measured from the base to the highest peak. When mice had
390 developed papillomas with a volume of ≥17 mm^3, the animals were stratified by papilloma size and
391 assigned into five groups with similar average tumor volumes (≈40 mm^3). Trametinib (Selleckchem) and
392 Cobimetinib (Selleckchem) in vehicle mixture (30% PEG-300 + 5% DMSO + 5% Tween-80 in dH_2O) were
393 administered by oral gavage and tumor dimensions and body weights were recorded every 48 h. Efficacy
394 was measured as percent tumor growth inhibition (TGI) relative to the vehicle-treated group. TGI was
395 calculated by the equation [1-(*T/C*) x 100], where *T* and *C* represent the mean tumor volumes on day 30
396 in the MEK inhibitor-treated (T) and vehicle control (C) groups, respectively. A TGI of >50% is considered
397 to be efficacious. On day 30, mice were euthanized by CO_2 exposure and whole tail sections receiving
398 the MmuPV1 inoculation were excised to include ≈0.5 cm of uninfected length on each side of the wart
399 growth. Tail sections were fixed in 4% paraformaldehyde (PFA) in PBS overnight at 4°C. Thereafter, each
400 tail section was rinsed twice with sterile PBS and incubated with Versenate decalcifying reagent (StatLab)
401 at 4°C until the tail bone became pliable. Tail sections were rinsed with sterile PBS and stored in 70%

402 ethanol at 4°C until paraffin-embedding. Muzzle papillomas were excised and stored in 4% PFA in PBS
403 overnight before washing twice with PBS and storing in 70% ethanol until paraffin-embedding.

404

405 **MmuPV1 infections *in vitro*.** HaCaT cells were seeded at 10^4 cells per plate in DMEM with 10% fetal calf
406 serum and allowed to adhere overnight at 37°C in 5% CO_2. Cells were pretreated for 1h with medium
407 containing vehicle (0.1% DMSO) or 1.0 to 100 nM trametinib prior to and during MmuPV1 exposure at
408 1000 VGE per cell. Infections proceeded for 48h before harvesting for total DNase I-treated RNA.
409 Following reverse transcription (RT), qPCR was performed using primers to amplify spliced MmuPV1
410 E1^E4 cDNA and normalized to ribosomal protein 18s mRNA levels as previously described (32, 83, 84).

411

412 **Tissue Staining and Immunohistochemistry (IHC).** Formalin-fixed paraffin embedded (FFPE) tail
413 sections and muzzle specimens 4-5 µm in thickness were baked at 60°C for 1 h. The Ventana Discovery
414 platform was used for deparaffinization, rehydration and H & E staining or blocking of endogenous
415 peroxidases for IHC. Antigens were unmasked by boiling in RiboCC buffer (Ventana 760-107; for keratin
416 10 and myeloperoxidase) for 32 min at 100°C. Antibodies to cytokeratin 10 (abcam ab76318; 1:250),
417 cytokeratin 5 (abcam ab52635; 1:400), and myeloperoxidase (abcam ab208670; 1:1000) were individually
418 diluted in Discovery PSS Diluent (Ventana 760-212), hand applied, and incubated for 16-32 min at 36°C.
419 Antibody incubation was followed by anti-Rb HQ (Ventana 760-4815), anti-HQ HRP (Ventana 760-4820),
420 and DAB CM (Ventana 760-4304) detection. Immunohistochemical detection of p-ERK1/2 (Cell Signaling
421 #4370; 1:500) required the tyramide signal amplification (TSA) biotin system following the manufacturer's
422 protocol (AKOYA Biosciences #NEL 700A001KT). Slides were counterstained with hematoxylin (Ventana
423 760-2021) and Bluing solution (Ventana 760-2037) or with Gill No.1 Hematoxylin solution (Sigma-Aldrich
424 #GHS132-1L) followed by acid alcohol and lithium carbonate rinse. Following dehydration, coverslips were
425 mounted using Permount (Fisher Scientific SP15-500). Stained slides were scanned at 20X using the Leica
426 Versa 200 digital slide scanner (Leica Biosystems, Buffalo Grove, IL).

427

428 **DNA and RNA *in situ* hybridization (ISH).** FFPE tail sections were stained according to the RNAscope
429 manufacturer's protocol (2.5 HD Detection Kit-Red, Advanced Cell Diagnostics [ACD]) using probes to
430 detect MmuPV1 E6/E7 RNA (ACD). DNA ISH employed probes to the noncoding MmuPV1 LCR Probe
431 (ACD) using the chromogenic DNAscope HD Kit. Slides were counterstained with 50% Gill's hematoxylin
432 solution number 1 (G Biosciences), mounted using EcoMount (BioCare Medical), and digitally imaged as
433 above.

434

435 **Immunofluorescence.** FFPE tail sections were deparaffinized, rehydrated, and subjected to heat-
436 induced antigen retrieval for 30 min using pH 9 target retrieval solution (Dako). Endogenous peroxidases
437 were blocked with 3% hydrogen peroxide in methanol for 10 min. Tissues were blocked with 5% goat
438 serum in PBS containing 0.1% Tween-20 (PBS-T) for 1 h at room temperature, then incubated at 4°C
439 overnight with rabbit sera against MmuPV1 L1 (a kind gift form Chris Buck, NIH; 1:2500) and chicken anti-
440 keratin 14 (BioLegend 905301; 1:500) diluted in 5% goat serum in PBS-T. The sections were then washed
441 three times in PBS-T followed by incubation with secondary antibodies (1:500) Alexa fluor (AF)-488 goat
442 anti-rabbit IgG (ThermoFisher A32731) and AF-647 goat anti-chicken IgG (ThermoFisher A32933) for 1 h
443 at room temperature. Coverslips were mounted using ProLong Diamond Antifade DAPI Mountant (Thermo
444 Fisher). Images were acquired using a Leica TCS SP8 confocal microscope with fixed data acquisition
445 settings. L1-positive foci were counted using Huygens essential software object analysis tool (Scientific
446 Volume Imaging, The Netherlands, http://svi.nl).

447

448 **Morphometric Tissue Analysis.** Tissue morphometry was performed on digitally acquired images from
449 all tumors using HALO software (Indica, Albuquerque, NM), under the supervision of a board-certified
450 veterinary pathologist (Kusewitt). The thickness of the epithelium within each lesion was determined using
451 H&E sections. The linear length of the lesion was measured, and HALO was trained to recognize all

452 epithelial elements lying above the dermis, then the area of epithelium within the lesion was determined.
453 The epithelium within each region was selected using the bucket tool; the selection was refined using the
454 line and scissors tools to include all nucleated cells and to eliminate artifacts. Within the identified
455 epithelium, stroma was identified and eliminated from consideration. Epithelial thickness was expressed
456 as the ratio of epithelial area to lesion length (mm). Using the CytoNuclear algorithm, individual epithelial
457 cells were identified and cytoplasmic staining for each marker was categorized as negative, low, medium,
458 or high. The total number of cells examined was enumerated and the percentage of epithelial cells staining
459 at each intensity was determined (e.g., *SI Appendix* Fig. S3A-C). As the ISH staining lacked sufficient
460 nuclear demarcation, total areas positive for ISH signals were determined. Neutrophil infiltration was
461 quantified by selecting all lesional epithelium and underlying dermis by hand. The percentage of that area
462 occupied by myeloperoxidase-positive neutrophils was determined using HALO software to identify and
463 quantify the area of positive staining. IHC stained slides were excluded from analysis (no more than one
464 per treatment group) if they lacked clear evidence of tail features that ensured the tumor was adequately
465 represented.

466

467 **Statistical Analyses**. Morphometry analyses included data from 5-6 tumors per group subjected to one-
468 way analysis of variance (ANOVA) with Tukey's multiple comparison test. RT-qPCR data were analyzed
469 by one-way ANOVA with Dunnett's multiple comparisons test. Biomarker level correlation coefficients (r)
470 were calculated from morphometry data using Pearson's correlation analysis and computing a two-tailed
471 p value. Tumor measurements among the five treatment groups were analyzed at each time point using
472 the generalized least square (GLS) method to account for the unequal variances among the groups (*SI*
473 *Appendix* Table 1). Differences among tumor groups at 30 days post treatment were evaluated by ANOVA
474 with the Tukey HSD (honest significant difference) pairwise comparisons (*SI Appendix* Table 2). The rates
475 of tumor volume changes were estimated and compared using the linear mixed-effects model (LMM)
476 analysis (*SI Appendix* Tables 3 and 4).

477

Acknowledgments

This study was supported by the American Cancer Society Mission Boost Grant MBG-18-207-01-COUN (M.A.O.); and the US National Institutes of Health Grants: R21DE028652 (M.A.O.); T32AI07538, F31CA232536, UNMCCC Matching Support (A.J.L.); P30CA118100 (M.A.O.). We acknowledge support by the following University of New Mexico Comprehensive Cancer Center shared resources (NCI 2P30CA118100): Human Tissue Repository and Tissue Analysis, Animal Models, Biostatistics.

We are grateful to Dr. Paul Lambert and members of his lab for generously providing infectious stocks of MmuPV1, to Dr. Nagayasu Egawa for sharing his protocols for mouse tail scarification and infection, and Dr. Christopher Buck for sharing rabbit sera against MmuPV1 L1.

Abbreviations

Activator protein-1 (AP-1); Alexa fluor (AF); analysis of variance (ANOVA); dimethyl sulfoxide (DMSO); formalin-fixed paraffin embedded (FFPE); generalized least square (GLS); human papillomaviruses (HPVs); human papillomavirus (HPV); immunohistochemistry (IHC); inhibitory concentration 50 (IC_{50}); *in situ* hybridization (ISH); keratin 5 (K5); keratin 10 (K10); linear mixed-effects model (LMM); long control region (LCR); Dulbecco's modified Eagle's medium (DMEM); murine papillomavirus type 1 (MmuPV1); paraformaldehyde (PFA); phosphate-buffered saline (PBS); tumor growth inhibition (TGI); viral genome equivalents (VGE).

500 **References**

501 1. N. Egawa, K. Egawa, H. Griffin, J. Doorbar, Human Papillomaviruses; Epithelial Tropisms, and
502 the Development of Neoplasia. *Viruses* **7**, 3863-3890 (2015).

503 2. PaVE: Papillomavirus Episteme: http://pave.niaid.nih.gov/ (accessed on 12 April 2023).

504 3. C. de Martel, M. Plummer, J. Vignat, S. Franceschi, Worldwide burden of cancer attributable to
505 HPV by site, country and HPV type. *Int. J. Cancer* **141**, 664-670 (2017).

506 4. D. C. Beachler *et al.*, Multisite HPV16/18 Vaccine Efficacy Against Cervical, Anal, and Oral HPV
507 Infection. *J. Natl. Cancer Inst.* **108** (2016).

508 5. K. Canfell *et al.*, Mortality impact of achieving WHO cervical cancer elimination targets: a
509 comparative modelling analysis in 78 low-income and lower-middle-income countries. *Lancet*
510 **395**, 591-603 (2020).

511 6. D. E. Johnson *et al.*, Head and neck squamous cell carcinoma. *Nat. Rev. Dis. Prim.* **6**, 92-22
512 (2020).

513 7. M. Maiman, Management of cervical neoplasia in human immunodeficiency virus-infected
514 women. *J. Natl. Cancer Inst. Monographs* **1998**, 43-49 (1998).

515 8. D. Martin *et al.*, Anal squamous cell carcinoma - State of the art management and future
516 perspectives. *Cancer Treat. Rev.* **65**, 11-21 (2018).

517 9. P. L. Stern *et al.*, Therapy of human papillomavirus-related disease. *Vaccine* **30 Suppl 5**, F71-82
518 (2012).

519 10. A. M. Ouda *et al.*, HPV and Recurrent Respiratory Papillomatosis: A Brief Review. *Life (Basel)*
520 **11**, 1279 (2021).

521 11. M. Oren-Shabtai *et al.*, Topical and Systemic Retinoids for the Treatment of Genital Warts: A
522 Systematic Review and Meta-Analysis. *Dermatology (Basel)* **237**, 389-395 (2021).

523 12. N. D. Christensen, L. R. Budgeon, N. M. Cladel, J. Hu, Recent advances in preclinical model
524 systems for papillomaviruses. *Virus Res.* **231**, 108-118 (2017).

525 13. M. E. Spurgeon, P. F. Lambert, Mus musculus Papillomavirus 1: A New Frontier in Animal
526 Models of Papillomavirus Pathogenesis. *J. Virol.* **94**, e00002-00020 (2020).

527 14. N. Egawa, J. Doorbar, The low-risk papillomaviruses. *Virus Res.* **231**, 119-127 (2017).

528 15. A. A. McBride, Human papillomaviruses: diversity, infection and host interactions. *Nat. Rev.*
529 *Microbiol.* **20**, 95-108 (2021).

530 16. J. Doorbar *et al.*, The biology and life-cycle of human papillomaviruses. *Vaccine* **30 Suppl 5**, F55-
531 70 (2012).

532 17. J. M. Meyers, A. Uberoi, M. Grace, P. F. Lambert, K. Munger, Cutaneous HPV8 and MmuPV1 E6
533 Proteins Target the NOTCH and TGF-beta Tumor Suppressors to Inhibit Differentiation and
534 Sustain Keratinocyte Proliferation. *PLoS Pathog.* **13**, e1006171 (2017).

535 18. J. T. Thomas, W. G. Hubert, M. N. Ruesch, L. A. Laimins, Human papillomavirus type 31
536 oncoproteins E6 and E7 are required for the maintenance of episomes during the viral life cycle in
537 normal keratinocytes. *Proc. Natl. Acad. Sci.* **96**, 8449-8454 (1999).

538 19. E. R. Flores, H. B. L. Allen, D. Lee, P. F. Lambert, The human papillomavirus type 16 E7
539 oncogene is required for the productive stage of the viral life cycle. *J. Virol.* **74**, 6622-6631 (2000).

540 20. K. Hoppe-Seyler, F. Bossler, J. A. Braun, A. L. Herrmann, F. Hoppe-Seyler, The HPV E6/E7
541 Oncogenes: Key Factors for Viral Carcinogenesis and Therapeutic Targets. *Trends Microbiol.* **26**,
542 158-168 (2018).

543 21. A. Pal, R. Kundu, Human Papillomavirus E6 and E7: The Cervical Cancer Hallmarks and Targets
544 for Therapy. *Front. Microbiol.* **10**, 3116 (2019).

545 22. E. Goodwin, D. DiMaio, Repression of human papillomavirus oncogenes in HeLa cervical
546 carcinoma cells causes the orderly reactivation of dormant tumor suppressor pathways. *Proc.*
547 *Natl. Acad. Sci.* **97**, 12513-12518 (2000).

548 23. S. M. Horner, R. A. DeFilippis, L. Manuelidis, D. DiMaio, Repression of the Human Papillomavirus
549 E6 Gene Initiates p53-Dependent, Telomerase-Independent Senescence and Apoptosis in HeLa
550 Cervical Carcinoma Cells. *J. Virol.* **78**, 4063-4073 (2004).

551 24. T. Rampias, C. Sasaki, P. Weinberger, A. Psyrri, E6 and E7 gene silencing and transformed
552 phenotype of human papillomavirus 16-positive oropharyngeal cancer cells. *J. Natl. Cancer Inst.*
553 **101**, 412-423 (2009).

554 25. J. Zhou *et al.*, Inhibition of cervical cancer cell growth in vitro and in vivo by lentiviral-vector
555 mediated shRNA targeting the common promoter of HPV16 E6 and E7 oncogenes. *Antiviral Res.*
556 **98**, 305-313 (2013).

557 26. C. J. Lee *et al.*, Induction of senescence-like state and suppression of telomerase activity through
558 inhibition of HPV E6/E7 gene expression in cells immortalized by HPV16 DNA. *Exp. Cell Res.*
559 **277**, 173-182 (2002).

560 27. M. von Knebel Doeberitz, C. Rittmüller, H. zur Hausen, M. Dürst, Inhibition of tumorigenicity of
561 cervical cancer cells in nude mice by HPV E6-E7 anti-sense RNA. *Int. J. Cancer* **51**, 831-834
562 (1992).

563 28. N. Sima *et al.*, Antisense targeting human papillomavirus type 16 E6 and E7 genes contributes to
564 apoptosis and senescence in SiHa cervical carcinoma cells. *Gynecol. Oncol.* **106**, 299-304
565 (2007).

566 29. N. Sima *et al.*, RNA interference against HPV16 E7 oncogene leads to viral E6 and E7
567 suppression in cervical cancer cells and apoptosis via upregulation of Rb and p53. *Apoptosis* **13**,
568 273-281 (2008).

569 30. E. M. Kennedy *et al.*, Inactivation of the human papillomavirus E6 or E7 gene in cervical
570 carcinoma cells by using a bacterial CRISPR/Cas RNA-guided endonuclease. *J. Virol.* **88**, 11965-
571 11972 (2014).

572 31. K. Zheng *et al.*, The Reservoir of Persistent Human Papillomavirus Infection; Strategies for
573 Elimination Using Anti-Viral Therapies. *Viruses* **14**, 214 (2022).

574 32. A. J. Luna *et al.*, MEK/ERK Signaling is a Critical Regulator of High-Risk Human Papillomavirus
575 Oncogene Expression Revealing Therapeutic Targets for HPV-Induced Tumors. *PLoS Pathog.*
576 **17**, e1009216 (2021).

577 33. A. A. Samatar, P. I. Poulikakos, Targeting RAS-ERK signalling in cancer: promises and
578 challenges. *Nat. Rev. Drug Discov.* **13**, 928-942 (2014).

579 34. M. Curto, B. K. Cole, D. Lallemand, C.-H. Liu, A. I. McClatchey, Contact-dependent inhibition of
580 EGFR signaling by Nf2/Merlin. *J. Cell Biol.* **177**, 893-903 (2007).

581 35. A. I. McClatchey, A. S. Yap, Contact inhibition (of proliferation) redux. *Curr. Opin. Cell Biol.* **24**,
582 685-694 (2012).

583 36. F. A. Scholl *et al.*, Mek1/2 MAPK Kinases Are Essential for Mammalian Development,
584 Homeostasis, and Raf-Induced Hyperplasia. *Dev. Cell* **12**, 615-629 (2007).

585 37. J. Cursons *et al.*, Regulation of ERK-MAPK signaling in human epidermis. *BMC Syst. Biol.* **9**, 41-
586 41 (2015).

587 38. Y. D. Shaul, R. Seger, The MEK/ERK cascade: from signaling specificity to diverse functions.
588 *Biochim. Biophys. Acta.* **1773**, 1213-1226 (2007).

589 39. F. Catalanotti *et al.*, A MEK1-MEK2 heterodimer determines the strength and duration of the ERK
590 signal. *Nat. Struct. Mol. Biol.* **16**, 294-303 (2009).

591 40. A. Brunet, G. Pagès, J. Pouysségur, Growth factor-stimulated MAP kinase induces rapid
592 retrophosphorylation and inhibition of MAP kinase kinase (MEK1). *FEBS Lett.* **346**, 299-303
593 (1994).

594 41. B. Xu, J. L. Wilsbacher, T. Collisson, M. H. Cobb, The N-terminal ERK-binding site of MEK1 is
595 required for efficient feedback phosphorylation by ERK2 in vitro and ERK activation in vivo. *J.*
596 *Biol. Chem.* **274**, 34029-34035 (1999).

597 42. H. J. Schaeffer *et al.*, MP1: a MEK binding partner that enhances enzymatic activation of the
598 MAP kinase cascade. *Science* **281**, 1668-1671 (1998).

599 43. W. Kolch, Coordinating ERK/MAPK signalling through scaffolds and inhibitors. *Nat. Rev. Mol. Cell*
600 *Biol.* **6**, 827-837 (2005).

601 44. M. Roy, Z. Li, D. B. Sacks, IQGAP1 is a scaffold for mitogen-activated protein kinase signaling.
602 *Mol. Cell. Biol.* **25**, 7940-7952 (2005).

603 45. G. Yin, J. Haendeler, C. Yan, B. C. Berk, GIT1 functions as a scaffold for MEK1-extracellular
604 signal-regulated kinase 1 and 2 activation by angiotensin II and epidermal growth factor. *Mol.*
605 *Cell. Biol.* **24**, 875-885 (2004).

606 46. R.-Y. Liang *et al.*, MEK2 is a critical modulating mechanism to down-regulate GCIP stability and
607 function in cancer cells. *FASEB J.* **34**, 1958-1969 (2020).

608 47. S. Giroux *et al.*, Embryonic death of Mek1-deficient mice reveals a role for this kinase in
609 angiogenesis in the labyrinthine region of the placenta. *Curr. Biol.* **9**, 369-372 (1999).

610 48. L. F. Bélanger *et al.*, Mek2 is dispensable for mouse growth and development. *Mol. Cell. Biol.* **23**,
611 4778-4787 (2003).

612 49. H. Cho *et al.*, Apoptosis inhibitor-5 overexpression is associated with tumor progression and poor
613 prognosis in patients with cervical cancer. *BMC Cancer* **14**, 545 (2014).

614 50. W.-M. Wang, S.-Y. Wu, A.-Y. Lee, C.-M. Chiang, Binding site specificity and factor redundancy in
615 activator protein-1-driven human papillomavirus chromatin-dependent transcription. *J. Biol.*
616 *Chem.* **286**, 40974-40986 (2011).

617 51. Y. Cheng, H. Tian, Current Development Status of MEK Inhibitors. *Molecules (Basel)* **22**, 1551
618 (2017).

619 52. R. Reid *et al.*, Genital warts and cervical cancer. III. Subclinical papillomaviral infection and
620 cervical neoplasia are linked by a spectrum of continuous morphologic and biologic change.
621 *Cancer* **53**, 943-953 (1984).

622 53. T. A. Khavari, J. Rinn, Ras/Erk MAPK signaling in epidermal homeostasis and neoplasia. *Cell*
623 *Cycle* **6**, 2928-2931 (2007).

624 54. H. Alam, L. Sehgal, S. T. Kundu, S. N. Dalal, M. M. Vaidya (2011) Novel function of keratins 5
625 and 14 in proliferation and differentiation of stratified epithelial cells. in *Mol. Biol. Cell*, pp 4068-
626 4078.

627 55. L.-j. Zhang, "Keratins in Skin Epidermal Development and Diseases" in Keratin, M. Blumenberg,
628 Ed. (IntechOpen, London, 2018), pp. 10.5772/intechopen.79050.

629 56. J. P. Sundberg *et al.*, Immune status, strain background, and anatomic site of inoculation affect
630 mouse papillomavirus (MmuPV1) induction of exophytic papillomas or endophytic
631 trichoblastomas. *PLoS ONE* **9**, e113582 (2014).

632 57. M. E. Spurgeon *et al.*, A Novel In Vivo Infection Model To Study Papillomavirus-Mediated
633 Disease of the Female Reproductive Tract. *mBio* **10**, 607 (2019).

634 58. V. Yilmaz, P. Louca, L. Potamiti, M. Panayiotidis, K. Strati, A novel lineage-tracing mouse model
635 for studying early MmuPV1 infections. *eLife* **11**, e72638 (2022).

636 59. J. T. Keating *et al.*, Ki-67, cyclin E, and p16INK4 are complimentary surrogate biomarkers for
637 human papilloma virus-related cervical neoplasia. *Am. J. Surg. Pathol.* **25**, 884-891 (2001).

638 60. A. G. Gilmartin *et al.*, GSK1120212 (JTP-74057) Is an Inhibitor of MEK Activity and Activation
639 with Favorable Pharmacokinetic Properties for Sustained In Vivo Pathway Inhibition. *Clin. Cancer*
640 *Res.* **17**, 989-1000 (2011).

641 61. Y. Liu *et al.*, Cobimetinib Sensitizes Cervical Cancer to Paclitaxel via Suppressing Paclitaxel-
642 Induced ERK Activation. *Pharmacology* **107**, 398-405 (2022).

643 62. A. Gertych *et al.*, Effects of tissue decalcification on the quantification of breast cancer
644 biomarkers by digital image analysis. *Diagn. Pathol.* **9**, 213 (2014).

645 63. N. Coleman *et al.*, Immunological events in regressing genital warts. *Am. J. Clin. Pathol.* **102**,
646 768-774 (1994).

647 64. C. L. Trimble *et al.*, Human papillomavirus 16-associated cervical intraepithelial neoplasia in
648 humans excludes CD8 T cells from dysplastic epithelium. *J. Immunol.* **185**, 7107-7114 (2010).

649 65. Y. L. Woo *et al.*, Characterising the local immune responses in cervical intraepithelial neoplasia: a
650 cross-sectional and longitudinal analysis. *BJOG* **115**, 1616-1621 (2008).

651 66. A. Handisurya *et al.*, Strain-Specific Properties and T Cells Regulate the Susceptibility to
652 Papilloma Induction by Mus musculus Papillomavirus 1. *PLoS Pathog.* **10**, e1004314 (2014).

653 67. N. M. Cladel *et al.*, Mouse papillomavirus infection persists in mucosal tissues of an
654 immunocompetent mouse strain and progresses to cancer. *Sci. Rep.* **7**, 16932-16912 (2017).

655 68. J. Doorbar, The papillomavirus life cycle. *J. Clin. Virol.* **32S**, S7-S15 (2005).

656 69. H.-U. Bernard, Regulatory elements in the viral genome. *Virology* **445**, 197-204 (2013).

657 70. G. L. Disbrow *et al.*, Dihydroartemisinin Is Cytotoxic to Papillomavirus-Expressing Epithelial Cells
658 In vitro and In vivo. *Cancer Res.* **65**, 10854-10861 (2005).

659 71. L. C. Gunder *et al.*, Efficacy of Topically Administered Dihydroartemisinin in Treating
660 Papillomavirus-Induced Anogenital Dysplasia in Preclinical Mouse Models. *Viruses* **14** (2022).

661 72. C. L. Trimble *et al.*, A first-in-human proof-of-concept trial of intravaginal artesunate to treat
662 cervical intraepithelial neoplasia 2/3 (CIN2/3). *Gynecol. Oncol.* **157**, 188-194 (2020).

663 73. J. R. da Silva *et al.*, Single immunizations of self-amplifying or non-replicating mRNA-LNP
664 vaccines control HPV-associated tumors in mice. *Sci. Transl. Med.* **15**, eabn3464 (2023).

665 74. M. A. Fuse *et al.*, Preclinical assessment of MEK1/2 inhibitors for neurofibromatosis type 2-
666 associated schwannomas reveals differences in efficacy and drug resistance development. *Neuro*
667 *Oncol.* **21**, 486-497 (2019).

668 75. K. P. Hoeflich *et al.*, Intermittent administration of MEK inhibitor GDC-0973 plus PI3K inhibitor
669 GDC-0941 triggers robust apoptosis and tumor growth inhibition. *Cancer Res.* **72**, 210-219
670 (2012).

671 76. G. A. Maglennon, P. B. McIntosh, J. Doorbar, Immunosuppression facilitates the reactivation of
672 latent papillomavirus infections. *J. Virol.* **88**, 710-716 (2014).

673 77. G. Dreyer, Clinical implications of the interaction between HPV and HIV infections. *Best Pract.*
674 *Res. Clin. Obstet. Gynaecol.* **47**, 95-106 (2018).

675 78. J. Doorbar, Host control of human papillomavirus infection and disease. *Best Pract. Res. Clin.*
676 *Obstet. Gynaecol.* **47**, 27-41 (2018).

677 79. A. Weiss, D. R. Littman, Signal transduction by lymphocyte antigen receptors. *Cell* **76**, 263-274
678 (1994).

679 80. T. Nakayama, M. Yamashita, The TCR-mediated signaling pathways that control the direction of
680 helper T cell differentiation. *Sem. Immunol.* **22**, 303-309 (2010).

681 81. N. V. Lieske, K. Tonby, D. Kvale, A. M. Dyrhol-Riise, K. Tasken, Targeting Tuberculosis and HIV
682 Infection-Specific Regulatory T Cells with MEK/ERK Signaling Pathway Inhibitors. *PLoS One* **10**,
683 e0141903 (2015).

684 82. V. Verma *et al.*, MEK inhibition reprograms CD8(+) T lymphocytes into memory stem cells with
685 potent antitumor effects. *Nat. Immunol.* **22**, 53-66 (2021).

686 83. N. Egawa *et al.*, Dynamics of Papillomavirus In Vivo Disease Formation & Susceptibility to High-
687 level Disinfection. Implications for Transmission in Clinical Settings. *EBioMedicine* **63**, 103177
688 (2021).

689 84. J. M. Young *et al.*, Protamine Sulfate Is a Potent Inhibitor of Human Papillomavirus Infection *In*
690 *Vitro* and *in Vivo*. *Antimicrob. Agents Chemother.* **66**, e01513-01521 (2022).

691

692 **Figures and Tables**

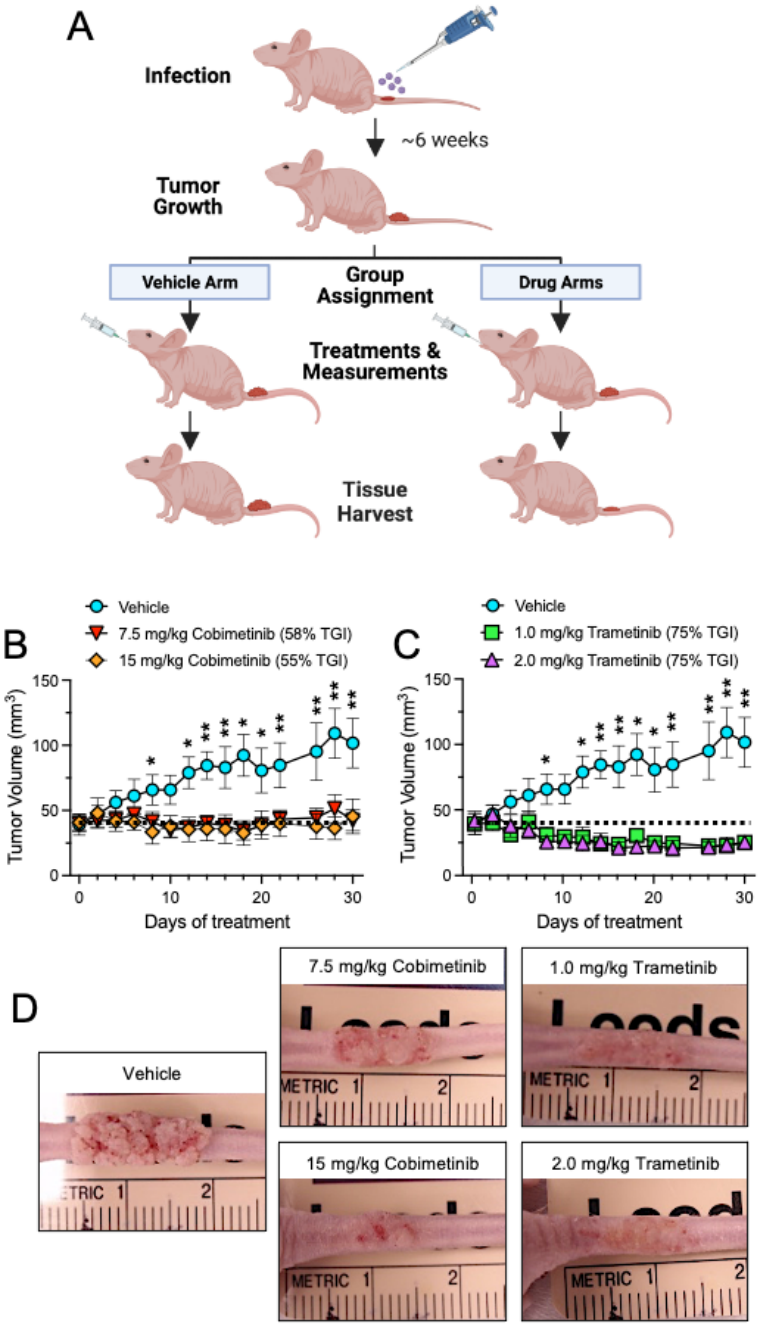

693

694 **Figure 1. MEK inhibition impairs MmuPV1-induced papilloma growth.** (A) Immediately after epithelial tail
695 scarification, female Hsd:Athymic Nude-*Foxn1*^{nu} mice were exposed to 2x10^{8} vge of MmuPV1. Papillomas were
696 allowed to grow for 6 weeks before assigning the animals into vehicle or treatment groups with similar average tumor
697 volumes (n=6 animals per group). Mice were treated by oral gavage treatment every 48h before harvesting the tumor-
698 bearing tail sections on day 30 post treatment. Image created with BioRender.com. (B, C) Mean tumor volumes
699 tracked over the treatment period with (B) cobimetinib or (C) trametinib (the vehicle group was the same for both
700 drugs). The dotted horizontal line marks the mean starting volumes. Data were analyzed comparing all treatment
701 groups together using ANOVA with the generalized least square method (*p<0.05 and **p<0.01; *SI Table 1*); the
702 treatments were graphed separately for clarity. Error bars represent SE. Mean TGI for the MEK inhibitors were 58%
703 and 55% for the 7.5 mg/kg and 15 mg/kg cobimetinib, respectively and 75% for both doses of trametinib. (D)
704 Representative images of the MmuPV1 induced papillomas for each treatment group at day 30 post treatment
705 initiation.

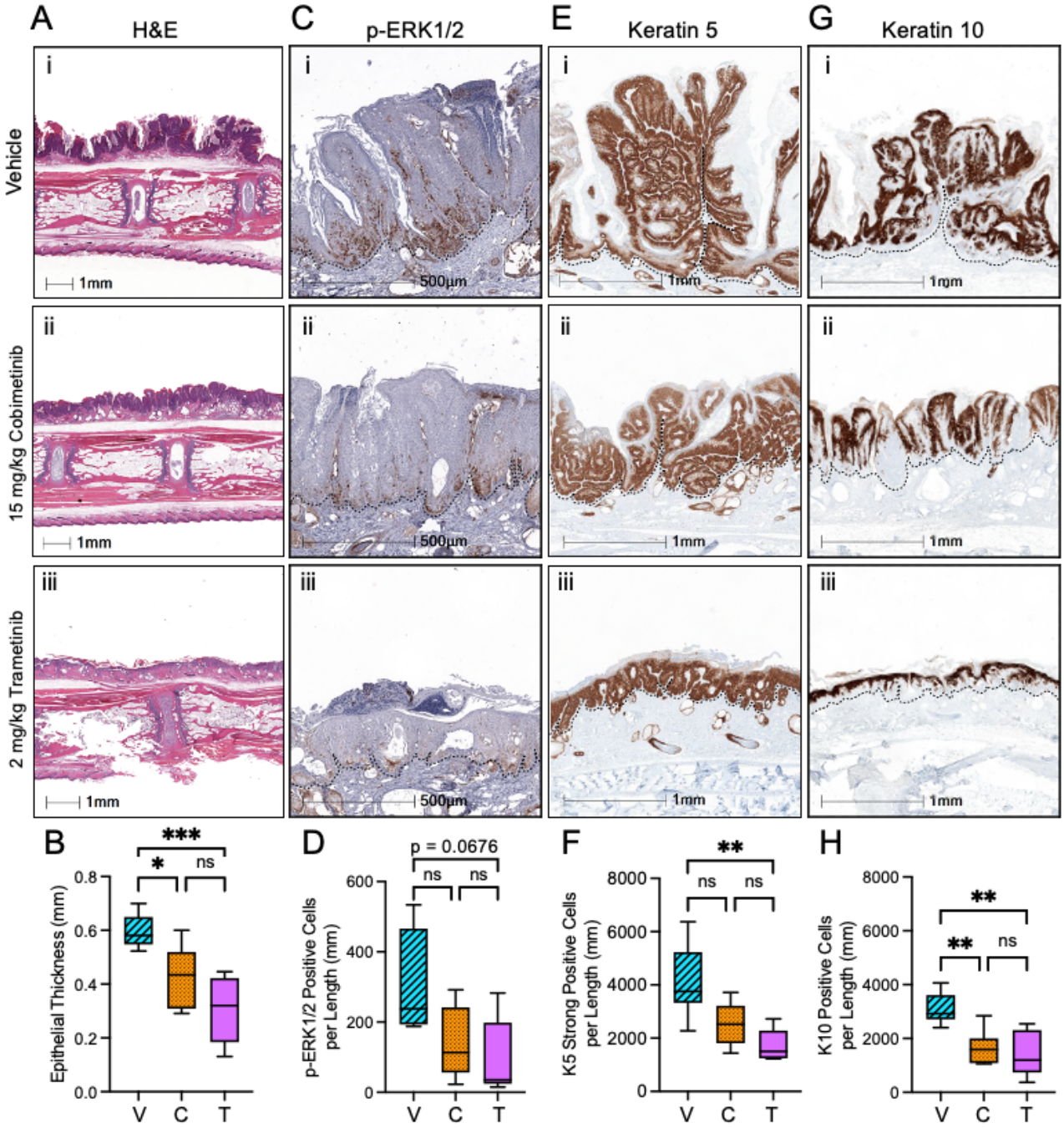

Figure 2. Histological and immunohistochemical analysis of MmuPV1-induced papillomas. Representative images of papilloma histology from mice treated with vehicle (i),15 mg/kg cobimetinib (ii), or 2.0 mg/kg trametinib (iii). Tails were fixed with paraformaldehyde, paraffin embedded, sectioned, and stained: (A) H&E; (C) IHC for p-ERK1/2; (E) IHC for keratin 5 (K5); (G) IHC for keratin 10 (K10); dotted lines mark the basement membrane. (B, D, F, H) Morphometric quantification of tail tumors from each mouse (4-5 per group) for papilloma thickness (height, B); p-ERK1/2 (D), K5 (F), and K10 (H) IHC staining expressed as positive cells per tumor length (mm); vehicle (V), 15 mg/ml cobimetinib (C), 2.0 mg/kg trametinib (T). Data were analyzed using one-way ANOVA with Tukey's multiple comparison test (*p<0.05, **p<0.01; ***p<0.001).

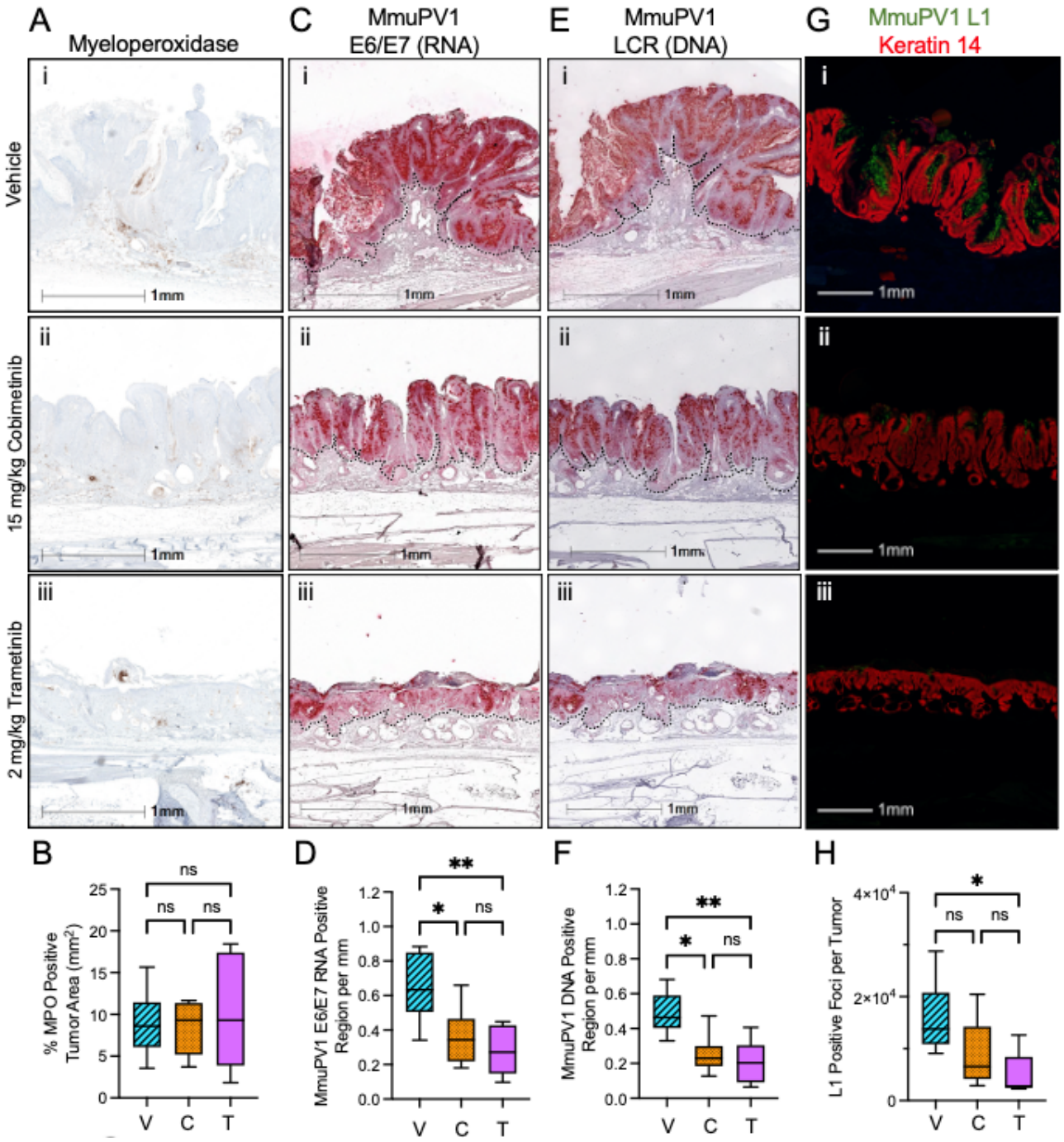

Figure 3. Histological analysis of immune and viral markers in MmuPV1-induced papillomas. Representative images of fixed histological papilloma sections for mice treated with vehicle (i),15 mg/kg cobimetinib (ii), or 2.0 mg/kg trametinib (iii). Tissues were stained *via*: (A) IHC for neutrophil marker, myeloperoxidase (MPO); (C) ISH for MmuPV1 E6/E7 mRNA; (E) ISH for MmuPV1 genomic DNA (note serial sections in panels C and E for comparison); (G) IF for MmuPV1 L1 protein (green) and keratin 14 (red). The brightness of the photos in panel G was enhanced equivalently to better illustrate L1 staining. (B, D, F, H) Morphometric quantification of each tumor section (vehicle, V; 15 mg/ml cobimetinib, C; 2.0 mg/kg trametinib, T) on raw images (n = 5-6/group) for the percent of MPO positive cells in the tumor (B), region of positive E6/E7 ISH staining per mm of papilloma (D), region of positive LCR ISH staining per mm of papilloma (F), and number of L1 positive foci per tumor (H). Data were analyzed using one-way ANOVA with Tukey's multiple comparison test (*p<0.05, **p<0.01).

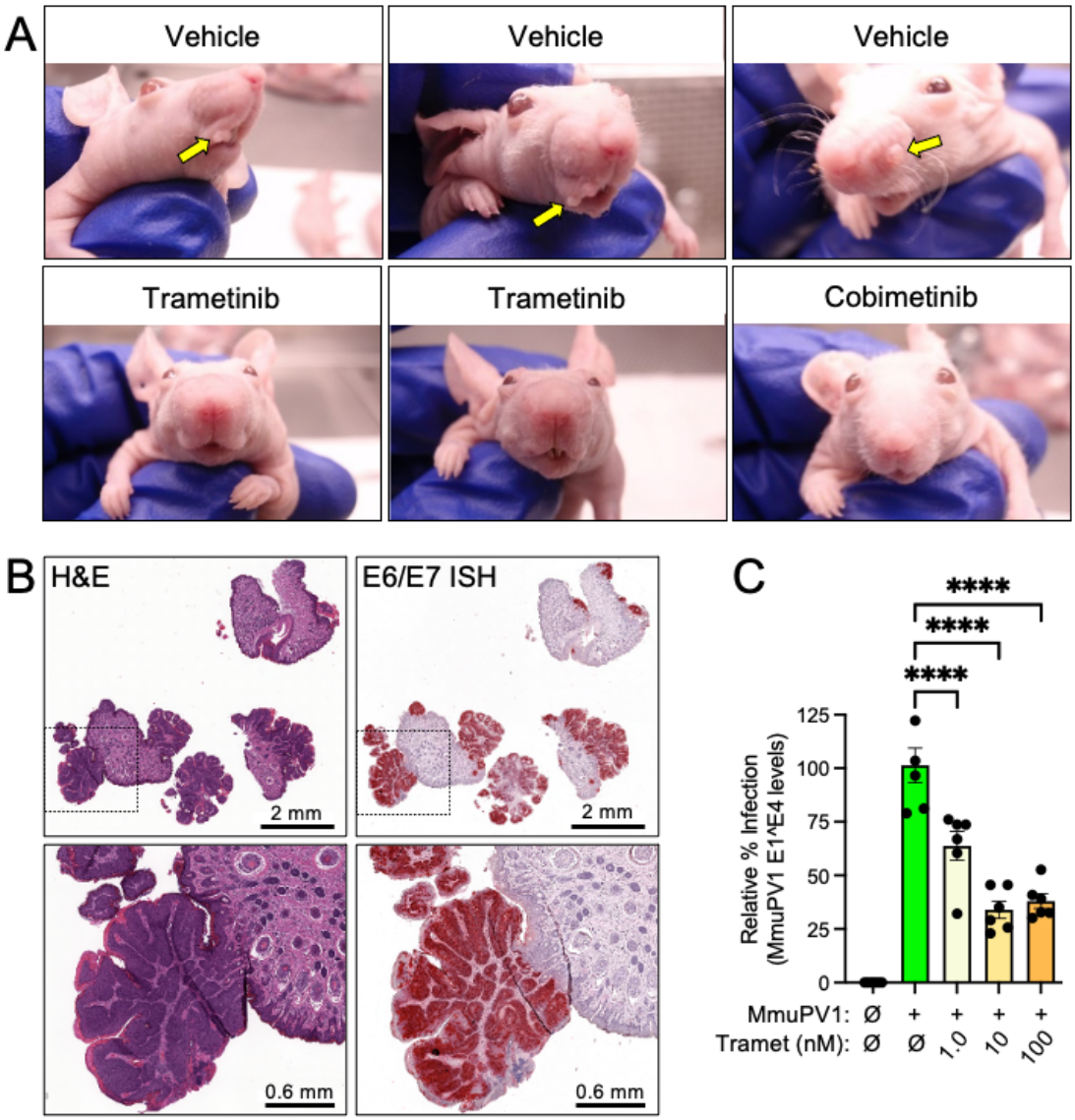

728

729

730 **Figure 4. MEK inhibition provides protection against MmuPV1 transmission to secondary epithelial**
731 **sites.** (A) Mice that were co-housed throughout the 30-day treatment period; arrows indicate papillomas
732 that developed on the muzzles of vehicle-treated mice. (B) Histological images of facial papillomas
733 harvested on day 30 post treatment. Tissue sections were stained with H&E or by MmuPV1 E6/E7 ISH.
734 Smaller boxes in upper panels indicate regions of increased magnification (lower panels). (C) Relative
735 MmuPV1 infection in untreated cells compared to those treated with increasing concentrations of
736 trametinib. Data summarize three independent infections analyzed by one-way ANOVA with Dunnett's
737 multiple comparisons test (**** $p<0.0001$).

738 **Table 1. Summary of animals developing visible muzzle warts**

Group	Wart positive mice / group total	Percentage
Vehicle	6/6	100%
7.5 mg/kg Cobimetinib	1/6	16.7%
15 mg/kg Cobimetinib	0/6	0%
1.0 mg/kg Trametinib	0/6	0%
2.0 mg/kg Trametinib	0/6	0%

739

Supplementary Information for

Inhibition of Cellular MEK/ERK Signaling Suppresses Murine Papillomavirus Type 1 Replicative Activities and Promotes Tumor Regression

Adrian J. Luna, Jesse M. Young, Rosa T. Sterk, Virginie Bondu, Fred A. Schultz,
Donna F. Kusewitt, Huining Kang, Michelle A. Ozbun

Corresponding author: Michelle A. Ozbun
Email: mozbun@salud.unm.edu

This PDF file includes:

Figures S1 to S5

Tables S1 to S4

Other supplementary materials for this manuscript include the following:

None

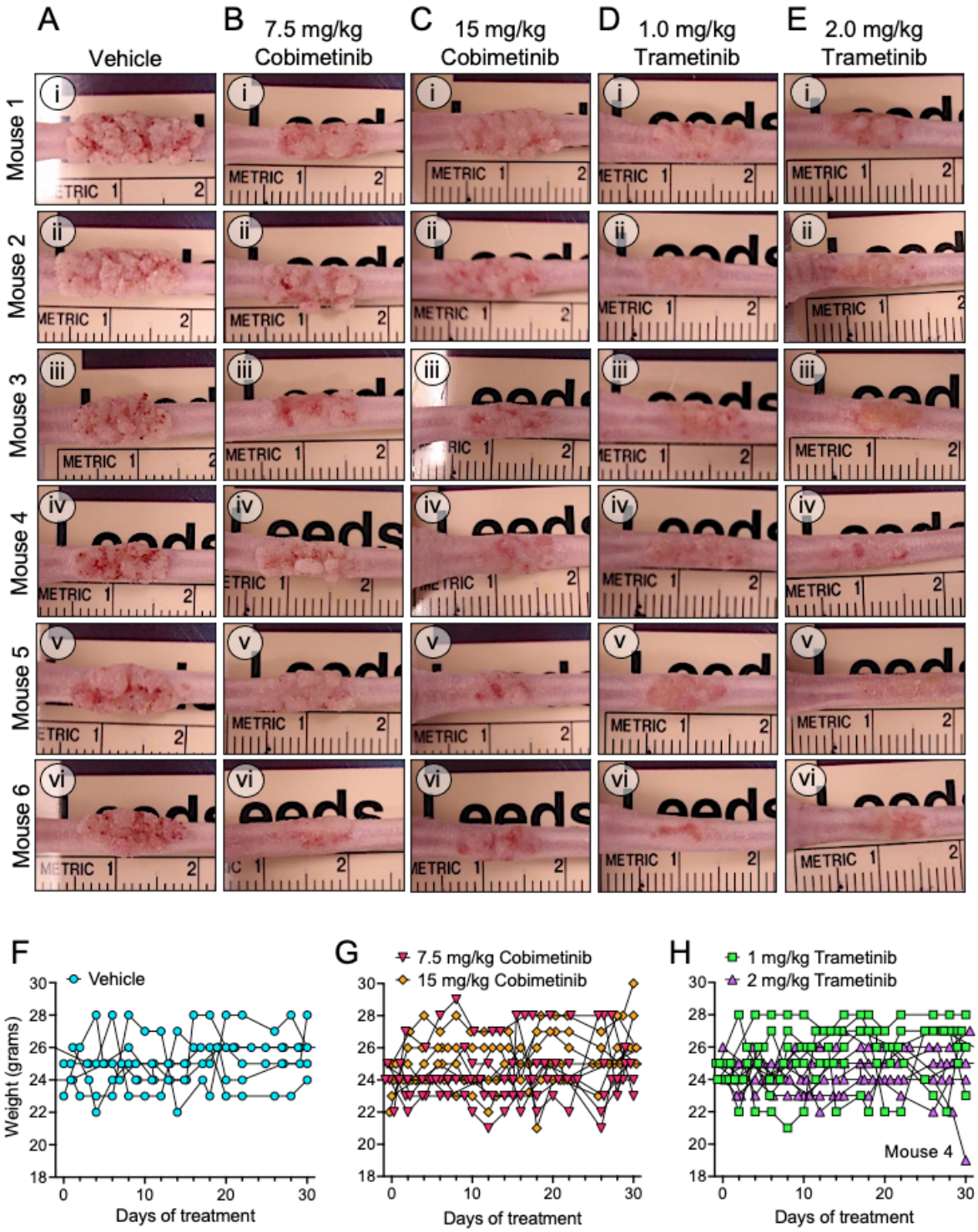

Fig. S1. Visual phenotypes of MmuPV1-induced papillomas at day 32 post treatment (prior to harvest). MmuPV1-induced papillomas after treatment with vehicle (A), 7.5 mg/kg cobimetinib (B), 15 mg/kg cobimetinib (C), 1 mg/kg trametinib (D), or 2 mg/kg trametinib (E). The labels at the left identify animal numbers in each treatment group. (F-H) Mouse weights during treatment period. Note that only one animal (mouse 4 of the 2 mg/kg trametinib treatment arm) showed substantial weight loss (>20% of starting weight).

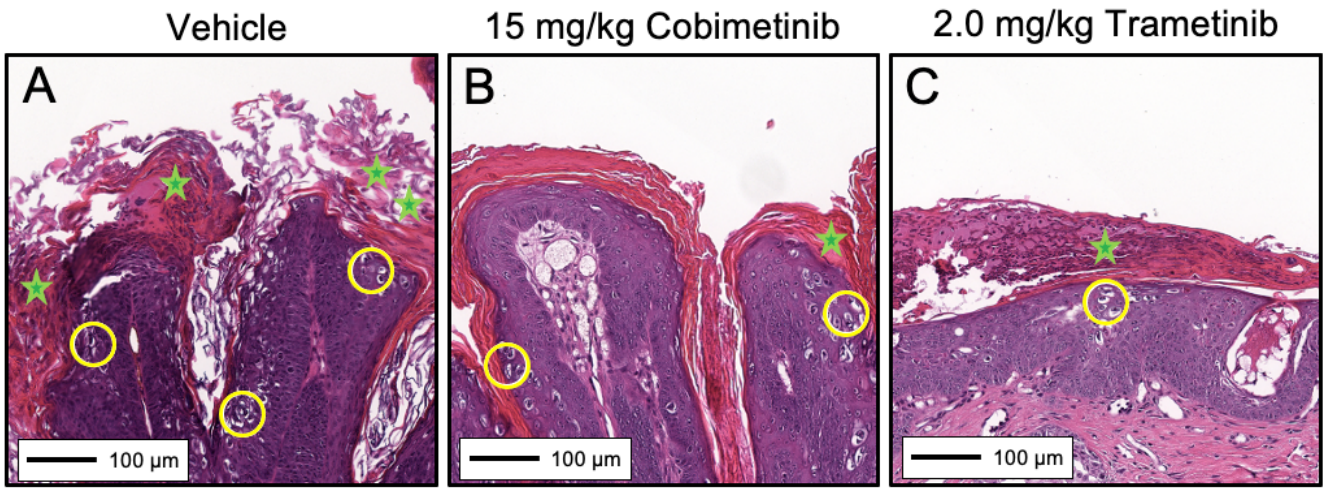

Fig. S2. Histologic features of MmuPV1-induced papillomas. High-magnification images of H&E-stained papillomatous tissue sections from animals treated with vehicle (A), 15 mg/kg cobimetinib (B) or 2.0 mg/kg trametinib (C). Regions of hyperkeratosis are denoted with green stars. Koilocytes, a hallmark of papillomavirus infections, are encircled in yellow.

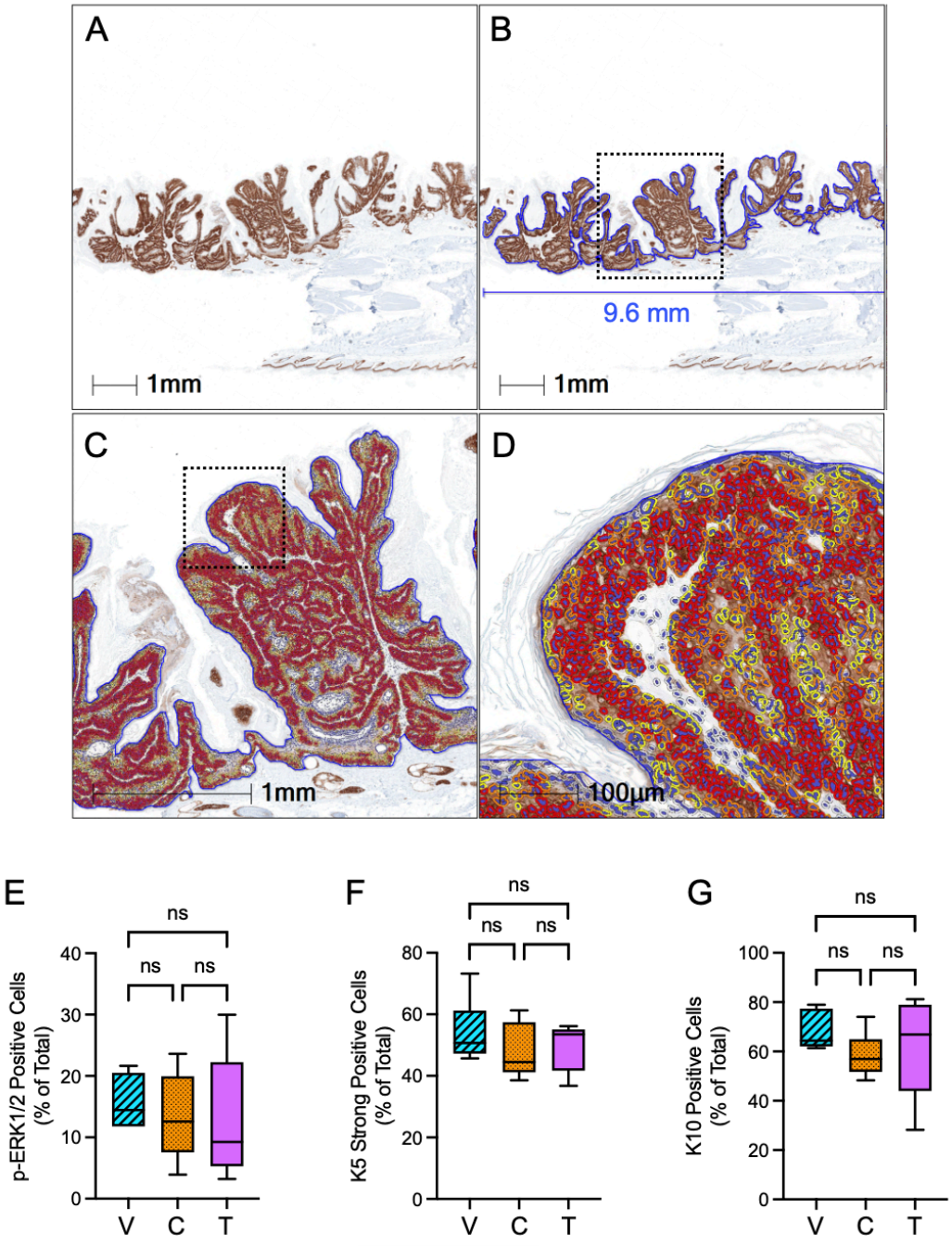

Fig. S3. Example of pathologist-guided morphometric analysis using a HALO algorithm to identify and quantify the areas of strong positive K5 staining and comparisons of % biomarker signals amongst the tumor groups. (A-B) Tumor-bearing areas were selected (blue) and defined as nuclei-containing epithelium; the boxed area in B was subject to increased magnification in panel C. (C) Using the CytoNuclear algorithm, individual epithelial cells were identified *via* marking nuclei blue and cytoplasmic staining for each marker was categorized as negative (clear), low (yellow), medium (orange), or high (red). (D) Increased magnification of the boxed area in panel C. Because cells gradually loose K5 expression as they begin to differentiate and express K10, only the strong K5 positive cells were enumerated. (E-G) Summary of morphometric analyses for the percentage of MmuPV1-induced tumors cells expressing the cellular proteins p-ERK1/2 (E), strong K5 (F), and K10 (G) for mice treated with vehicle (V), 15 mg/ml cobimetinib (C), 2 mg/kg trametinib (T). Data were analyzed using one-way ANOVA with Tukey's multiple comparison test (ns = not significant).

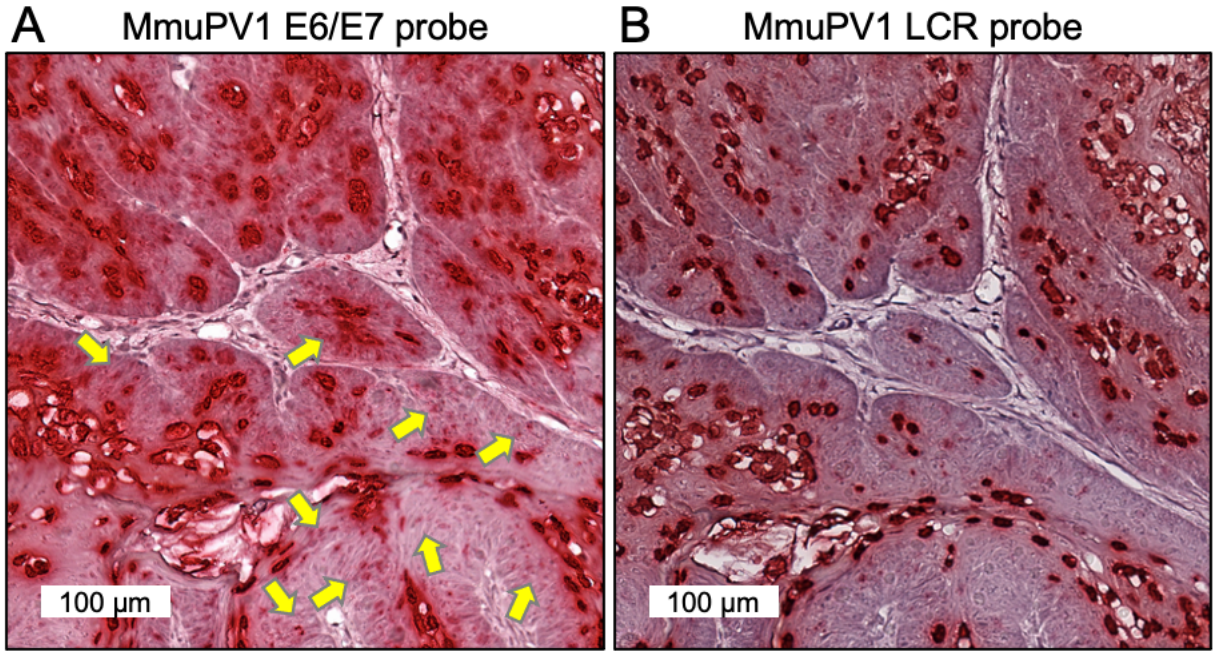

Fig. S4. Magnified images of ISH using probes specific for the MmuPV1 E6/E7 coding region (A) and the noncoding genomic LCR segment (B) in adjacent tumor sections from a vehicle-treated mouse. Note that both probes strongly stained nuclei in koilocytes and suprabasal cells likely to be amplifying viral genomes. Whereas the E6/E7 probes demonstrated cytoplasmic punctate signals expected for viral mRNAs (A, yellow arrows), the LCR probe produced little cytoplasmic signal (B).

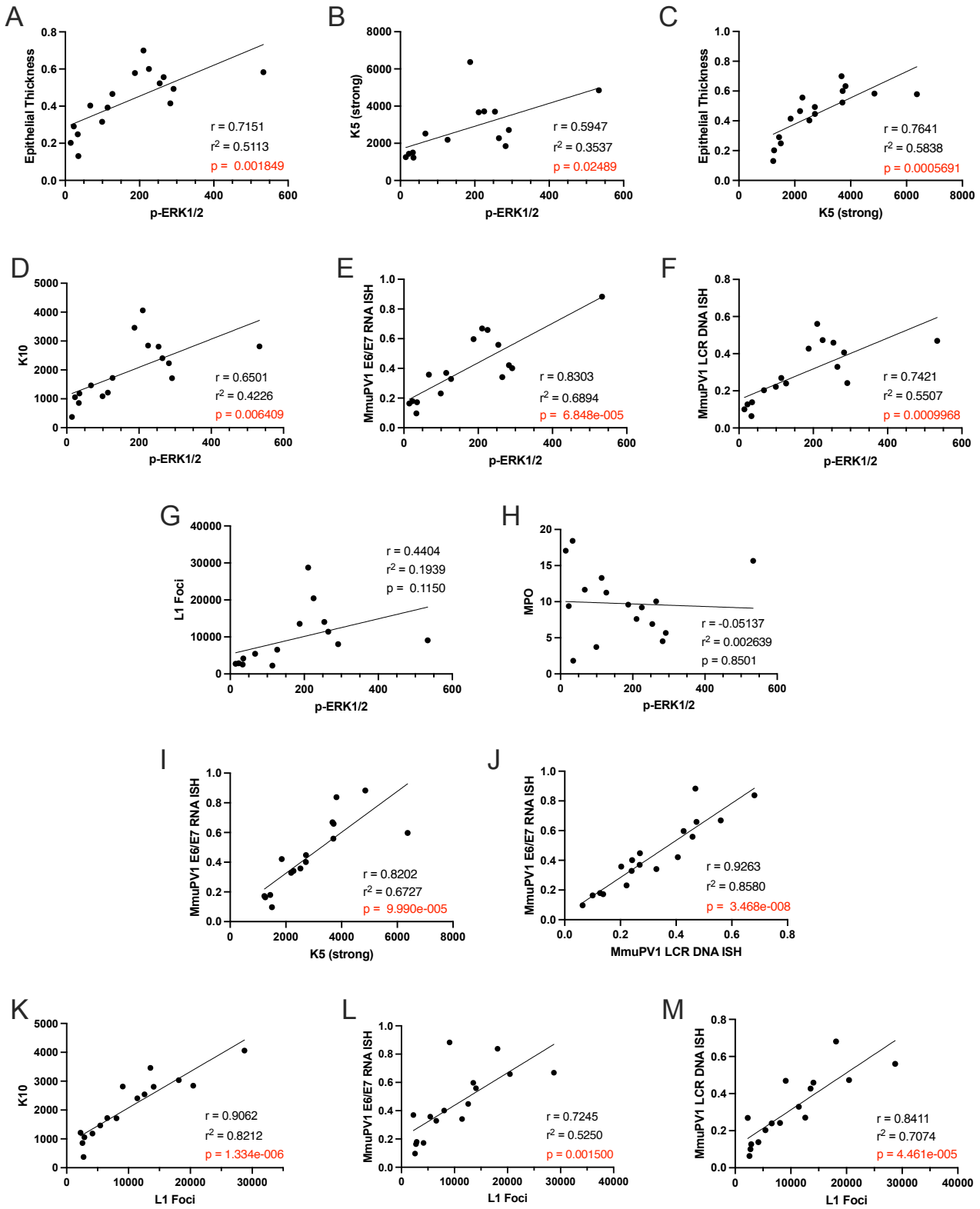

Fig. S5. MEK inhibitor reduced tissue levels of p-ERK1/2 correlate with cellular and viral biomarkers in MmuPV1-induced tail tumors. Scatter dot plot correlations analyses between selected biomarkers were calculated using Pearson correlation coefficient (r) analysis and a two-tailed test (p values). P values that reached statistical significance are shown in red.

SI Table 1. Mean and Standard Error (SE) of Tumor Volumes (mm^3)

Time (days)	**Vehicle** Mean (SE)	**7.5 mg/kg Cobimetinib** Mean (SE)	**15 mg/kg Cobimetinib** Mean (SE)	**1.0 mg/kg Trametinib** Mean (SE)	**2.0 mg/kg Trametinib** Mean (SE)	**p-value**[a]
0	39.2 (8.1)	39.8 (6.3)	40.8 (6.3)	39.3 (8.0)	41.6 (7.5)	0.998996
2	46.8 (7.1)	42.1 (5.4)	48 (11.6)	40.1 (6.1)	46.1 (7.5)	0.906252
4	56.1 (9.0)	42.6 (5.8)	41.9 (7.9)	31.1 (5.5)	37.8 (8.7)	0.20922
6	61.2 (12.8)	47.0 (4.4)	41.1 (6.0)	40.9 (8.3)	34.3 (6.3)	0.27487
8	65.8 (11.6)	41.5 (7.5)	33.5 (9.2)	30.9 (5.9)	25.5 (4.3)	0.041988
10	65.8 (11.2)	34.9 (5.9)	37.8 (8.3)	29.5 (5.1)	26.0 (5.4)	0.069824
12	78.9 (12.2)	36.9 (4.6)	35.5 (9.3)	29.1 (7.7)	24.5 (6.0)	0.023779
14	84.5 (10.6)	40.3 (5.7)	36.0 (9.2)	24.1 (4.0)	25.9 (6.2)	0.001759
16	82.9 (16.0)	38.5 (5.3)	35.7 (11)	23.5 (4.4)	20.9 (4.4)	0.005515
18	92.3 (16.0)	34.0 (6.6)	32.7 (9.5)	30.3 (3.7)	21.8 (4.3)	0.016097
20	80.7 (17.1)	38.3 (6.9)	39.0 (10.7)	24.8 (5.1)	22.4 (3.7)	0.015508
22	84.7 (17.3)	43.2 (6.2)	40.0 (10.0)	24.4 (4.5)	20.7 (6.1)	0.004064
24	95.2 (22.1)	44.4 (7.3)	37.7 (9.8)	22.5 (2.6)	21.4 (4.5)	0.004354
28	109.2 (19.2)	51.4 (10.7)	36.4 (8.8)	22.6 (4.6)	23.2 (5.8)	0.002729
30	101.7 (19.1)	42.4 (8.0)	45.4 (13.2)	25.0 (4.4)	25.2 (4.8)	0.00718

[a] p-value for the significance of the difference in tumor volume among the five groups obtained using GLS to account for unequal variances.

SI Table 2. Pairwise Comparisons of Final Tumor Volumes Among Treatment Groups at 30 Days of Treatment

Treatment 1	Treatment 2	Difference[a]	Lower[b]	Upper[c]	p-value adj[d]
1.0 mg/kg Trametinib	Vehicle	-76.7042163	-88.255000	-65.15343	0.0005834
2.0 mg/kg Trametinib	Vehicle	-76.4767450	-88.027529	-64.92596	0.0006047
7.5 mg/kg Cobimetinib	Vehicle	-59.2767633	-70.827547	-47.72598	0.0087560
15 mg/kg Cobimetinib	Vehicle	-56.2683900	-67.819174	-44.71761	0.0137132
2.0 mg/kg Trametinib	1.0 mg/kg Trametinib	0.2274713	-11.323313	11.77826	1.0000000
7.5 mg/kg Cobimetinib	1.0 mg/kg Trametinib	17.4274530	5.876669	28.97824	0.8121645
15 mg/kg Cobimetinib	1.0 mg/kg Trametinib	20.4358263	8.885042	31.98661	0.7095422
7.5 mg/kg Cobimetinib	2.0 mg/kg Trametinib	17.1999817	5.649198	28.75077	0.8192129
15 mg/kg Cobimetinib	2.0 mg/kg Trametinib	20.2083550	8.657571	31.75914	0.7178020
15 mg/kg Cobimetinib	7.5 mg/kg Cobimetinib	3.0083733	-8.542411	14.55916	0.9997039

[a] The difference in tumor volumes between the pair of the groups
[b] The lower bounds of the 95% confidence interval (CI)
[c] The upper bounds of the 95% confidence interval (CI)
[d] The adjusted p-value for testing the significance of the difference between the two treatments in columns one and two. The results indicate that the difference between Vehicle and each of the groups with the MEK inhibitor is significant (adj. p-value < 0.05). But there is no significant difference when comparing between any of the groups that received the MEK inhibitor, as none of the corresponding p-values is less than 0.05.

SI Table 3. Estimates for Rates of Change of Tumor Volumes (Slope)

Group	Estimate[a]	SE[b]	DF[c]	t-value[d]	p-value[e]
Vehicle	1.849	0.615	445	3.01	0.0028
1 mg/kg Trametinib	-0.4739	0.2262	445	-2.09	0.0368
2 mg/kg Trametinib	-0.5325	0.254	445	-2.1	0.0366
7.5 mg/kg Cobimetinib	0.1011	0.2795	445	0.36	0.7178
15 mg/kg Cobimetinib	0.1168	0.3679	445	0.32	0.7509

[a] Estimates for the rate of change (mm^3/day) derived from the slopes of the linear equations
[b] The standard error (SE)
[c] The degree of freedom (DF)
[d] The value of t-test (t-value) where the t-test investigates whether the corresponding slopes are zero.
[e] The p-value investigates whether the rate of change significantly differs from zero.

SI Table 3 shows the estimates for the rate of change (mm^3/day), the slopes of the linear equations of the five groups, along with the SE, DF, t-value and p-value. The t-test here investigates whether the corresponding slopes are zero. The p-values in the first three rows are all smaller than 0.05, suggesting that the rate of change of tumors in the vehicle-treated mice and of tumors in mice treated with trametinib significantly differ from zero. The tumor volumes in vehicle-treated mice significantly increased over time (because the corresponding slope is positive), and that of groups treated with trametinib significantly decreased over time (as the corresponding slopes are negative). The tumor volumes in groups treated with cobimetinib have the smallest estimates for the slopes (in the sense of the absolute value), and the corresponding p-values are very large, indicating that the rate of change is not significantly different from zero (i.e., the tumor volumes, on average, did not have a significant change over time).

SI Table 4. Difference in Rates of Change of Tumor Volumes (Slope)

Difference in Rate of Change	**Estimate[a]**	**SE[b]**	**DF[c]**	**t-value[d]**	**p-value[e]**
Between Vehicle and 1 mg/kg Trametinib	2.3229	0.6553	445	3.54	0.0004
Between Vehicle and 2 mg/kg Trametinib	2.3816	0.6654	445	3.58	0.0004
Between Vehicle and 7.5 mg/kg Cobimetinib	1.7479	0.6756	445	2.59	0.01
Between Vehicle and 15 mg/kg Cobimetinib	1.7322	0.7167	445	2.42	0.016
Between Vehicle and Overall Treatment	2.0462	0.6315	445	3.24	0.0013
Between Two Doses of Trametinib	0.05866	0.3402	445	0.17	0.8631
Between Two Doses of Cobimetinib	-0.01576	0.462	445	-0.03	0.9728
Between Trametinib and Cobimetinib	-0.6122	0.2869	445	-2.13	0.0334

[a] Estimates for difference in the rate of change (mm^3/day) between the two groups of interest obtained based on the LMM
[b] The standard error (SE)
[c] The degree of freedom (DF)
[d] The value of t-test (t-value) where the t-test investigates whether the corresponding differences are zero.
[e] The p-value investigates whether the rate of change significantly differs between the groups of interest.

SI Table 4 shows the analysis of the individual tumor rates of change for each treatment group using the linear mixed-effects model (LMM). Based on the fitted LMM, we estimated the differences in the rate of change for comparisons of interest. The first four rows provide the estimates for the difference in the rate of change between the Vehicle and each MEK inhibitor treatment group. The fact that the p-values are smaller than 0.05 indicates that the rate of change differs significantly between each pair of the groups. The fifth row shows the comparison between the Vehicle and overall treatment group (the union of all the treatment groups), and a small p-value implies that the difference in the rate of change is significant. These results provide statistical evidence for the considerable effect of MEK inhibitors on tumor growth. In rows six and seven, we compared the dose effect on the rate of change among the same drug, and the large p-values indicate that the dose effect is insignificant. Lastly, we compared the difference in the rate of change between the two drugs regardless of the dose. The result indicates a significant difference in the rate of change between those treated with the two drugs (p-value = 0.0334).